

THEORETICAL FOUNDATIONS OF t-SNE FOR VISUALIZING HIGH-DIMENSIONAL CLUSTERED DATA

T. Tony Cai¹ and Rong Ma²

Department of Statistics¹

Department of Biostatistics, Epidemiology and Informatics²

University of Pennsylvania

Philadelphia, PA 19104

Abstract

This study investigates the theoretical foundations of t-distributed stochastic neighbor embedding (t-SNE), a popular nonlinear dimension reduction and data visualization method. A novel theoretical framework for the analysis of t-SNE based on the gradient descent approach is presented. For the early exaggeration stage of t-SNE, we show its asymptotic equivalence to a power iteration based on the underlying graph Laplacian, characterize its limiting behavior, and uncover its deep connection to Laplacian spectral clustering, and fundamental principles including early stopping as implicit regularization. The results explain the intrinsic mechanism and the empirical benefits of such a computational strategy. For the embedding stage of t-SNE, we characterize the kinematics of the low-dimensional map throughout the iterations, and identify an amplification phase, featuring the intercluster repulsion and the expansive behavior of the low-dimensional map. The general theory explains the fast convergence rate and the exceptional empirical performance of t-SNE for visualizing clustered data, brings forth the interpretations of the t-SNE output, and provides theoretical guidance for selecting tuning parameters in various applications.

KEY WORDS: Clustering; Data visualization; Foundation of data science; Nonlinear dimension reduction; t-SNE

1 Introduction

Data visualization is critically important for understanding and interpreting the structure of large data sets, and has been recognized as one of the fundamental topics in data science (Donoho, 2017). A collection of machine learning algorithms for data visualization and dimension reduction have been developed. Among them, the t-distributed stochastic neighbor embedding (t-SNE) algorithm,

proposed by van der Maaten and Hinton (2008), is arguably the most popular procedure and a state-of-art technique in a wide range of applications (Wang et al., 2020).

Specifically, t-SNE is an iterative algorithm for visualizing high-dimensional data by mapping the data points to a two- or three-dimensional space. It creates a single map that reveals the intrinsic structures in a high-dimensional dataset, including trends, patterns, and outliers, through a nonlinear dimension reduction technique. In the past decade, the original t-SNE algorithm, along with its many variants (for example, Yang et al. (2009); Carreira-Perpinán (2010); Xie et al. (2011); van der Maaten (2014); Gisbrecht et al. (2015); Pezzotti et al. (2016); Im et al. (2018); Linderman et al. (2019); Chatzimparmpas et al. (2020)), has made profound impact to the practice of scientific research, including genetics (Platzer, 2013), molecular biology (Olivon et al., 2018), single-cell transcriptomics (Kobak and Berens, 2019), computer vision (Cheng et al., 2015) and astrophysics (Traven et al., 2017). In particular, the extraordinary performance of t-SNE for visualizing high-dimensional data with intrinsic clusters has been widely acknowledged (van der Maaten, 2014; Kobak and Berens, 2019).

Compared to the extensive literature on the computational and numerical aspects of t-SNE, there is a paucity of fundamental results about its theoretical foundations (see Section 1.3 for a brief overview). The lack of theoretical understanding and justifications profoundly limits the users' interpretation of the results as well as the potentials for further improvement of the method.

This paper aims to investigate the theoretical foundations of t-SNE. Specifically, we present a novel framework for the analysis of t-SNE, provide theoretical justifications for its competence in dimension reduction and visualizing clustered data, and uncover the fundamental principles underlying its exceptional empirical performance.

1.1 The Basic t-SNE Algorithm

Let $\{X_i\}_{1 \leq i \leq n}$ be a set of p -dimensional data points. t-SNE starts by computing a joint probability distribution over all pairs of data points $\{(X_i, X_j)\}_{1 \leq i \neq j \leq n}$, represented by a symmetric matrix $\mathbf{P} = (p_{ij})_{1 \leq i,j \leq n} \in \mathbb{R}^{n \times n}$, where $p_{ii} = 0$ for all $1 \leq i \leq n$, and for $i \neq j$,

$$p_{ij} = \frac{p_{i|j} + p_{j|i}}{2n} \quad \text{with} \quad p_{j|i} = \frac{\exp(-\|X_i - X_j\|_2^2/2\tau_i^2)}{\sum_{\ell \in \{1, 2, \dots, n\} \setminus \{i\}} \exp(-\|X_i - X_\ell\|_2^2/2\tau_i^2)}. \quad (1)$$

Here τ_i are tuning parameters, which are usually determined based on a certain perplexity measure and a simple binary search (Hinton and Roweis, 2002; van der Maaten and Hinton, 2008). Similarly, in a two-dimensional map $\{y_i\}_{1 \leq i \leq n} \subset \mathbb{R}^2$, define the joint probability distribution over all pairs $\{(y_i, y_j)\}_{1 \leq i \neq j \leq n}$ through a symmetric matrix $\mathbf{Q} = (q_{ij})_{1 \leq i,j \leq n}$ where $q_{ii} = 0$ for all $1 \leq i \leq n$ and for $i \neq j$,

$$q_{ij} = \frac{(1 + \|y_i - y_j\|_2^2)^{-1}}{\sum_{\ell, s \in \{1, 2, \dots, n\}, \ell \neq s} (1 + \|y_\ell - y_s\|_2^2)^{-1}}. \quad (2)$$

Intuitively, \mathbf{P} and \mathbf{Q} are similarity matrices summarizing the pairwise distances of the high-dimensional data points $\{X_i\}_{1 \leq i \leq n}$, and the two-dimensional map $\{y_i\}_{1 \leq i \leq n}$, respectively. Then t-SNE aims to find $\{y_i\}_{1 \leq i \leq n}$ in \mathbb{R}^2 that minimizes the KL-divergence between \mathbf{P} and \mathbf{Q} , that is,

$$(y_1, \dots, y_n) = \arg \min_{y_1, \dots, y_n} D_{KL}(\mathbf{P}, \mathbf{Q}) = \arg \min_{y_1, \dots, y_n} \sum_{i, j \in \{1, 2, \dots, n\}, i \neq j} q_{ij} \log \frac{p_{ij}}{q_{ij}}. \quad (3)$$

Many algorithms have been proposed to solve this optimization problem. The most widely used algorithm was proposed by van der Maaten and Hinton (2008), which draws on a variant of gradient descent algorithm, with an updating equation

$$y_i^{(k+1)} = y_i^{(k)} + h D_i^{(k)} + m^{(k+1)} (y_i^{(k)} - y_i^{(k-1)}), \quad \text{for } i = 1, \dots, n, \quad (4)$$

where $h \in \mathbb{R}_+$ is a prespecified step size parameter, $D_i^{(k)} = 4 \sum_{1 \leq j \leq n, j \neq i} (y_j^{(k)} - y_i^{(k)}) S_{ij}^{(k)} \in \mathbb{R}^2$ is the gradient term corresponding to y_i , with $S_{ij}^{(k)} = (p_{ij} - q_{ij}^{(k)}) / (1 + \|y_i^{(k)} - y_j^{(k)}\|_2^2) \in \mathbb{R}$, and $m^{(k)} \in \mathbb{R}_+$ is a prespecified momentum parameter. The algorithm starts with an initialization $y_i^{(0)} = y_i^{(-1)}$ for $i \in \{1, 2, \dots, n\}$, drawn independently from $N(0, \delta^2 I)$ for some small $\delta > 0$.

As indicated by van der Maaten and Hinton (2008), the inclusion of the momentum term $m^{(k+1)} (y_i^{(k)} - y_i^{(k-1)})$ in (4) is mainly to speed up the convergence and to reduce the risk of getting stuck in a local minimum. In this paper, for simplicity and generality we focus on the basic version of the t-SNE algorithm based on the simple gradient descent, with the updating equation

$$y_i^{(k+1)} = y_i^{(k)} + h D_i^{(k)}, \quad \text{for } i = 1, \dots, n. \quad (5)$$

In van der Maaten and Hinton (2008) and van der Maaten (2014), the recommended total number of iterations is 1000, while the step size h is initially set as 400 or 800, and is updated at each iteration by an adaptive learning rate scheme of Jacobs (1988).

The standard gradient descent algorithm as in (5) suffers from a slow convergence rate and even non-convergence in some applications. As an amelioration, van der Maaten and Hinton (2008) proposed an *early exaggeration* technique, applied to the initial stages of the optimization, that helps to create patterns in the visualization and speed up the convergence. Such a computational strategy has been standard in practical use. In general, most of the current software implementations of t-SNE are based on an early exaggeration stage followed by an embedding stage that iterates a certain gradient descent algorithm. In our setting, these two stages can be summarized as follows.

Early exaggeration stage. For the first $K_0 > 0$ iterations, the p_{ij} 's in the gradient term $D_i^{(k)}$ are multiplied by some exaggeration parameter $\alpha > 0$, so the updating equation for this early

exaggeration stage becomes

$$y_i^{(k+1)} = y_i^{(k)} + h \sum_{1 \leq j \leq n, j \neq i} (y_j^{(k)} - y_i^{(k)}) S_{ij}^{(k)}(\alpha), \quad i = 1, \dots, n, \quad (6)$$

where $S_{ij}^{(k)}(\alpha) = (\alpha p_{ij} - q_{ij}^{(k)}) / (1 + \|y_i^{(k)} - y_j^{(k)}\|_2^2) \in \mathbb{R}$, and the factor 4 in $D_i^{(k)}$ is absorbed into the step size parameter h . We refer to this first stage of the t-SNE algorithm as the *early exaggeration stage*.

In van der Maaten and Hinton (2008), the authors choose $\alpha = 4$ and $K_0 = 50$ for the early exaggeration stage, whereas later in van der Maaten (2014), it is recommended that $\alpha = 12$ and $K_0 = 250$. In particular, it is empirically observed that, the early exaggeration technique enables t-SNE to find a better global structure in the early stages of the optimization by creating very tight clusters of points that easily move around in the embedding space (van der Maaten, 2014); this observation is later supported by some pioneering theoretical investigations (see Section 1.3). Nevertheless, there are interesting questions to be answered concerning (i) the underlying principles and mechanism behind such a computational strategy, (ii) the limit behavior of the low-dimensional map, (iii) how sensitive is the performance of t-SNE with respect to the choice of (α, h, K_0) , and (iv) how to efficiently determine the values of (α, h, K_0) in order to achieve the best empirical performance.

Embedding stage. After the early exaggeration stage, the exaggeration parameter α is dropped and the original iterative algorithm (5) is carried out till attaining a prespecified number of steps. We refer to this second stage of the t-SNE algorithm as the *embedding stage*. The final output is a two-dimensional map $\{y_i^{(K_1)}\}_{1 \leq i \leq n}$, commonly treated as a low-dimensional embedding of the original high-dimensional data points $\{X_i\}_{1 \leq i \leq n}$, that preserves its global or local structures.

In addition to data visualization, t-SNE is sometimes also used as an intermediate step for clustering, signal detection, among many other purposes. In particular, it has been observed that, when applied to high-dimensional clustered data, t-SNE tends to produce a visualization with more separated clusters, which are often in good agreement with the clusters found by a dedicated clustering algorithm (Kobak and Berens, 2019). See Figure 1 for an example of data visualization using such a basic t-SNE algorithm.

1.2 Main Results and Our Contribution

A novel theoretical framework is introduced for the analysis of t-SNE, which relies on a joint statistical and computational analysis based on a double-index asymptotic scheme. More specifically, our asymptotic analysis concerns both the large sample limit, where the sample size goes to infinity, and the computational time limit, where the number of algorithmic iterations goes to infinity. Our main results may be summarized from three perspectives.

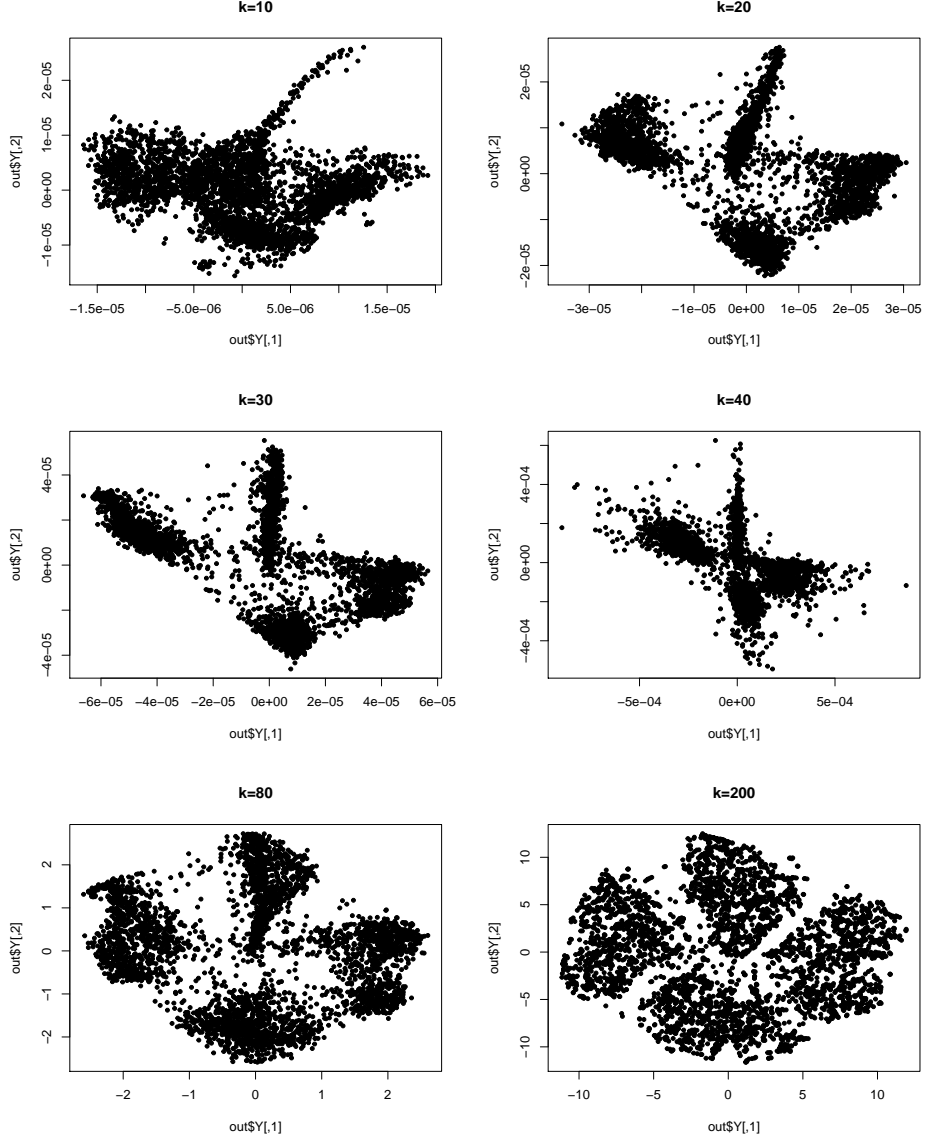


Figure 1: An illustration of the t-SNE iterations that visualize samples from the MNIST dataset (<http://yann.lecun.com/exdb/mnist/index.html>). Each data point is an image of one of the handwritten digits “2,” “4,” “6,” and “8.” The visualizations are obtained using the `Rtsne` function in the R package `Rtsne`, by selecting the exact t-SNE mode (`theta=0`, `pca=F`), dropping the momentum terms (`momentum=0`, `final_momentum = 0`), and setting `perplexity=30`, $\alpha = 12$ (default), $h = 200$ (default) in (6), and $K_0 = 40$. The first three plots (by row) correspond to the early exaggeration stage, while the last three plots correspond to the embedding stage.

The early exaggeration stage. Through a discrete-time analysis, we establish the asymptotic equivalence between the early exaggeration stage and a power iteration based on the underlying graph Laplacian associated with the high-dimensional data, providing a spectral-graphical inter-

pretation of the algorithm. We show the implicit spectral clustering mechanism at this stage, which explains the adaptivity and flexibility of t-SNE for visualizing clustered data without knowing the number of clusters. Specifically, for the case where $\{X_i\}_{1 \leq i \leq n}$ are clustered into R groups, we make the key observation that the coordinates of $\{y_i^{(k)}\}_{1 \leq i \leq n}$ converge to the R -dimensional Laplacian null space, leading to a limiting embedding where the elements of $\{y_i^{(k)}\}_{1 \leq i \leq n}$ corresponding to the same cluster are identical. On the other hand, through a continuous-time analysis, we study the underlying gradient flow and uncover the implicit regularization effect due to an early stopping of the iterations, which makes the method less susceptible to noises and to over-fitting. These analyses justify the empirical benefits of the early exaggeration technique in creating cluster structures and speeding up the algorithm.

The embedding stage. We provide a mechanical interpretation of the algorithm by characterizing the kinematics of the low-dimensional map at each iteration. Specifically, we identify an amplification phase within the embedding stage, featuring the local intercluster repulsion and the global expansive behavior of $\{y_i^{(k)}\}_{1 \leq i \leq n}$. In the former case, it is shown that the movement of each $y_i^{(k)}$ to $y_i^{(k+1)}$ is jointly determined by the repulsive forces pointing toward $y_i^{(k)}$ from each of the other clusters (Figure 2), that amounts to increasing spaces between the existing clusters; in the latter case, it is shown the diameter of $\{y_i^{(k)}\}_{1 \leq i \leq n}$ may strictly increase after each iteration. We observe that, following the amplification phase, there is a stabilization phase where $\{y_i^{(k)}\}_{1 \leq i \leq n}$ is locally adjusted to achieve a finer embedding of $\{X_i\}_{1 \leq i \leq n}$. These results together explain the fast convergence rate and the exceptional empirical performance of t-SNE for visualizing clustered data.

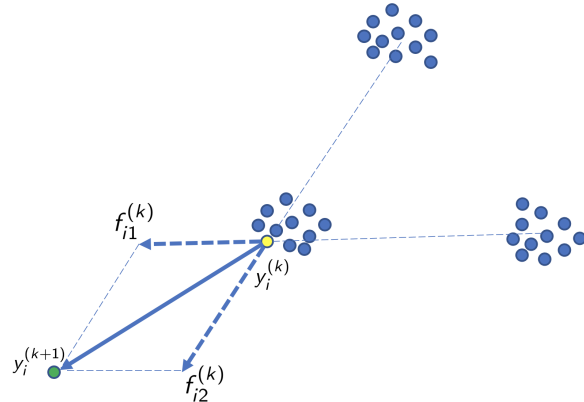


Figure 2: An illustration of the intercluster repulsion where the original data $\{X_i\}_{1 \leq i \leq n}$ have three clusters. The position of $y_i^{(k+1)}$ is jointly determined by $y_i^{(k)}$ and two repulsive forces $f_{i1}^{(k)}$ and $f_{i2}^{(k)}$ pushing $y_i^{(k)}$ away from the other two clusters not including $y_i^{(k)}$.

Practical implications. The general theory brings forth the interpretations of the t-SNE output, and provides theoretical guidance for selecting tuning parameters in various applications. In particular, our analysis unveils the roles of the tuning parameters in determining the visualization quality, which to some extent answers the question raised by Linderman and Steinerberger (2019). Finally, to demonstrate the theoretical and practical implications of our general results in different contexts, we apply our general theory to two concrete examples of high-dimensional clustered data, generated from a Gaussian mixture model, and a noisy nested sphere model, respectively.

1.3 Related Work

The impressive empirical performance of t-SNE has recently attracted much theoretical interests. Linderman and Steinerberger (2019) showed that, in the early exaggeration stage of t-SNE, with properly chosen parameters α and h , a subset of the two-dimensional map belonging to the same cluster will shrink in diameter, suggesting well-clustered visualization following iterations. In Shamam and Steinerberger (2017), a large family of methods including t-SNE as a special case were studied and shown to successfully map well-separated disjoint clusters from high dimensions to the real line so as to approximately preserve the clustering. In Arora et al. (2018), a theoretical framework was developed to formalize the notion of visualizing clustered data, which is used to analyze the early exaggeration stage of t-SNE, and to justify its high visualization quality. By extending the idea of t-SNE, Im et al. (2018) considered a class of methods with various loss functions based on the f -divergence, and theoretically assessed the performances of these methods based on a neighborhood-level precision-recall analysis. More recently, Zhang and Steinerberger (2021) proposed to view t-SNE as a force-based method which generates embeddings by balancing attractive and repulsive forces between data points. In particular, the limiting behavior of t-SNE was analyzed under a mean-field model where a single homogeneous cluster is present.

Despite these results, the theoretical understanding of t-SNE is still limited. Many intriguing phenomena and important features that arise commonly in practice have not been well understood or properly explained. Moreover, it remains unclear how to interpret the final visualization produced by t-SNE. These important questions are carefully addressed in the current work.

1.4 Notation and Organization

For a vector $\mathbf{a} = (a_1, \dots, a_n)^\top \in \mathbb{R}^n$, we denote $\text{diag}(a_1, \dots, a_n) \in \mathbb{R}^{n \times n}$ as the diagonal matrix whose i -th diagonal entry is a_i , and define the ℓ_p norm $\|\mathbf{a}\|_p = (\sum_{i=1}^n a_i^p)^{1/p}$. For a matrix $\mathbf{A} = (a_{ij}) \in \mathbb{R}^{n \times n}$, we define its Frobenius norm as $\|\mathbf{A}\|_F = \sqrt{\sum_{i=1}^n \sum_{j=1}^n a_{ij}^2}$, and its spectral norm as $\|\mathbf{A}\| = \sup_{\|\mathbf{x}\|_2 \leq 1} \|\mathbf{A}\mathbf{x}\|_2$; we also denote $\mathbf{A}_{\cdot i} \in \mathbb{R}^n$ as its i -th column and $\mathbf{A}_{i \cdot} \in \mathbb{R}^n$ as its i -th row. Let $O(n, k) = \{\mathbf{V} \in \mathbb{R}^{n \times k} : \mathbf{V}^\top \mathbf{V} = \mathbf{I}_k\}$ be the set of all $n \times k$ orthonormal matrices and $O_n = O(n, n)$, the set of n -dimensional orthonormal matrices. For a rank r matrix $\mathbf{A} \in \mathbb{R}^{n \times n}$ with $1 \leq r \leq n$, its eigendecomposition is denoted as $\mathbf{A} = \mathbf{U}\mathbf{\Sigma}\mathbf{U}^\top$ where $\mathbf{U} \in O(n, r)$

with its columns being the eigenvectors, and $\mathbf{\Gamma} = \text{diag}(\lambda_1(\mathbf{A}), \lambda_2(\mathbf{A}), \dots, \lambda_r(\mathbf{A}))$ with $\lambda_{\min}(\mathbf{A}) = \lambda_1(\mathbf{A}) \leq \dots \leq \lambda_n(\mathbf{A}) = \lambda_{\max}(\mathbf{A})$ being the ordered eigenvalues of \mathbf{A} . For a smooth function $f(x)$, we denote $\dot{f}(x) = df(x)/dx$ and $\ddot{f}(x) = d^2f(x)/dx^2$. For any integer $n > 0$, we denote the set $[n] = \{1, 2, \dots, n\}$. For a finite set S , we denote its cardinality as $|S|$. For a subset $S \subseteq \mathbb{R}^n$, we define its diameter $\text{diam}(S) = \sup_{x, y \in S} \|x - y\|_2$. For sequences $\{a_n\}$ and $\{b_n\}$, we write $a_n = o(b_n)$ or $a_n \ll b_n$ if $\lim_n a_n/b_n = 0$, and write $a_n = O(b_n)$, $a_n \lesssim b_n$ or $b_n \gtrsim a_n$ if there exists a constant C such that $a_n \leq Cb_n$ for all n . We write $a_n \asymp b_n$ if $a_n \lesssim b_n$ and $a_n \gtrsim b_n$. Throughout, C, C_1, C_2, \dots are universal constants, that can vary from line to line.

The rest of the paper is organized as follows. Section 2 presents the theoretical analysis for the early exaggeration stage of t-SNE. Section 3 analyzes the embedding stage. The general theory is then applied in Section 4 to two specific settings of model-based clustered data, one under a Gaussian mixture model and another under a noisy nested sphere model. Section 5 discusses potential applications, extensions and other related problems. Section 6 contains the proofs of some main theorems in Section 2. The proofs of other theorems are collected in Appendix.

2 Theoretical Analysis of the Early Exaggeration Stage

2.1 Asymptotic Graphical Interpretation and Localization

We start with a key observation that connects the updating equation (6) to some graph-related concepts. To this end, we introduce the following definition.

Definition 1 (Degree & Laplacian Operators). For a symmetric matrix $\mathbf{A} = (a_{ij})_{1 \leq i, j \leq n} \in \mathbb{R}^{n \times n}$, define the degree operator $\mathbf{D} : \mathbb{R}^{n \times n} \rightarrow \mathbb{R}^{n \times n}$ by $\mathbf{D}(\mathbf{A}) = \text{diag}(\sum_{i=1}^n a_{i1}, \dots, \sum_{i=1}^n a_{in})$, and the Laplacian operator $\mathbf{L} : \mathbb{R}^{n \times n} \rightarrow \mathbb{R}^{n \times n}$ by $\mathbf{L}(\mathbf{A}) = \mathbf{D}(\mathbf{A}) - \mathbf{A}$.

We define $\mathbf{S}_\alpha^{(k)} = (S_{ij}^{(k)}(\alpha))_{1 \leq i, j \leq n} \in \mathbb{R}^{n \times n}$ with $S_{ii}^{(k)}(\alpha) \equiv 0$ for all $i \in [n]$. Then we can rewrite the updating equation (6) using the matrix form as

$$\mathbf{y}_\ell^{(k+1)} = [\mathbf{I}_n - h\mathbf{L}(\mathbf{S}_\alpha^{(k)})]\mathbf{y}_\ell^{(k)}, \quad \ell = 1, 2, \quad (7)$$

where $\mathbf{I}_n \in \mathbb{R}^{n \times n}$ is the identity matrix, and $\mathbf{y}_\ell^{(k)} \in \mathbb{R}^n$ consists of the ℓ -th coordinates of $\{y_i^{(k)}\}_{1 \leq i \leq n}$. As a consequence, for each iteration k , if we treat the symmetric matrix $\mathbf{S}_\alpha^{(k)}$ as the adjacency matrix of a weighted graph $G^{(k)}$ with n nodes that summarizes the pairwise relationships between n data points $\{X_i\}_{1 \leq i \leq n}$, Equation (7) has an interpretation that links to the Laplacian matrix of such a weighted graph.

To better understand the meaning and the properties of the underlying graph $G^{(k)}$ that evolve over iterations, we take a closer look at its adjacency matrix $\mathbf{S}_\alpha^{(k)}$. In particular, one should keep in mind that in common applications of t-SNE, the early exaggeration stage has the following empirical features: (i) moderate or relatively large values of the exaggeration parameter α (default

12 in the R package `Rtsne`), (ii) local initializations $\{y_i^{(0)}\}_{1 \leq i \leq n}$ around the origin (see Section 1.1), and (iii) relative small diameters $\text{diam}(\{y_i^{(k)}\}_{1 \leq i \leq n})$ over iterations (Figure 1).

Our next result shows that, these empirical features of t-SNE have deep connections to the asymptotic behavior of the evolving underlying graphs and their adjacency matrices $\{\mathbf{S}_\alpha^{(k)}\}_{k \geq 1}$ in the large sample limit (as $n \rightarrow \infty$).

Theorem 1 (Asymptotic Graphical Interpretation). *Define $\eta^{(k)} = [\text{diam}(\{y_i^{(k)}\}_{1 \leq i \leq n})]^2$. For any $i, j \in [n]$ with $i \neq j$, and each $k \geq 1$ such that $\eta^{(k)} < 1$, we have*

$$\left| S_{ij}^{(k)}(\alpha) - \alpha p_{ij} + \frac{1}{n(n-1)} \right| \leq \alpha p_{ij} \eta^{(k)} + \frac{2\eta^{(k)}}{n(n-1)(1-\eta^{(k)})}. \quad (8)$$

Consequently, if we denote $\mathbf{1}_n = (1, \dots, 1)^\top \in \mathbb{R}^n$, and $\mathbf{H}_n = \frac{1}{n(n-1)}(\mathbf{1}_n \mathbf{1}_n^\top - \mathbf{I}_n)$, then for each $k \geq 1$, as long as $(\eta^{(k)}, \alpha)$ satisfies

$$\eta^{(k)} \ll \frac{\|\mathbf{P}\|}{n\|\mathbf{P}\|_\infty}, \quad \alpha \gg \frac{1}{n\|\mathbf{P}\|}, \quad \text{as } n \rightarrow \infty, \quad (9)$$

we have

$$\lim_{n \rightarrow \infty} \frac{\|\mathbf{S}_\alpha^{(k)} - (\alpha \mathbf{P} - \mathbf{H}_n)\|}{\|\alpha \mathbf{P} - \mathbf{H}_n\|} = 0. \quad (10)$$

The above theorem implies that, for large n , as long as the diameter of $\{y_i^{(k)}\}_{1 \leq i \leq n}$ remains sufficiently small and the exaggeration parameter α sufficiently large, the adjacency matrix $\mathbf{S}_\alpha^{(k)}$ behaves almost like a fixed matrix $\alpha \mathbf{P} - \mathbf{H}_n$ across the iterations. In other words, we may treat the updating equation (7) as an approximately linear equation

$$\mathbf{y}_\ell^{(k+1)} \approx [\mathbf{I}_n - h\mathbf{L}(\alpha \mathbf{P} - \mathbf{H}_n)]\mathbf{y}_\ell^{(k)}, \quad \ell = 1, 2, \quad (11)$$

where the linear operator $\mathbf{I}_n - h\mathbf{L}(\alpha \mathbf{P} - \mathbf{H}_n)$ only relies on the Laplacian of a fixed weighted graph whose adjacency matrix is given by the scaled and shifted similarity matrix $\alpha \mathbf{P} - \mathbf{H}_n$. This essentially opens the door to the key observation about the asymptotic equivalence between the early exaggeration stage and a power iteration.

Before we formally present such a result, we need to first point out an important phenomena concerning the global behavior of the low-dimensional map at the early exaggeration stage. Specifically, we make the following assumptions on the initialization and the tuning parameters (α, h, k) :

(I1) $\{y_i^{(0)}\}_{1 \leq i \leq n}$ satisfies $\min_{\ell \in [2]} \|\mathbf{y}_\ell^{(0)}\|_2 > 0$, and $\max_{\ell \in [2]} \|\mathbf{y}_\ell^{(0)}\|_\infty = O(1)$ as $n \rightarrow \infty$;
and

(T1) the parameters (α, h, k) satisfy $k(nh\alpha\|\mathbf{P}\|_\infty + h/n) = O(1)$ as $n \rightarrow \infty$.

Intuitively, Condition (I1) says that the initialization $\{y_i^{(0)}\}_{1 \leq i \leq n}$ should not be simply all zeros or unbounded, whereas the condition (T1) – as a consequence of (8) – essentially requires the cumulative deviations of $h\mathbf{L}(\mathbf{S}_\alpha^{(k)})$ from $h\mathbf{L}(\alpha\mathbf{P} - \mathbf{H}_n)$ to be bounded. Our next result shows that, under these assumptions, the diameter of $\{y_i^{(k)}\}_{1 \leq i \leq n}$ may not increase throughout the iterations, so the embedding remains localized within the initial range.

Proposition 1 (Localization). *Suppose (I1) and (T1) hold. We have*

$$\text{diam}(\{y_i^{(k+1)}\}_{1 \leq i \leq n}) \leq C \max_{\ell \in [2]} \|\mathbf{y}_\ell^{(0)}\|_\infty, \quad (12)$$

for some universal constant $C > 0$.

The above proposition confirmed the globally localized and non-expansive behavior of $\{y_i^{(k)}\}_{1 \leq i \leq n}$ over the early exaggeration stage observed in practice (Figure 1). Concerning Theorem 1, it tells us the step-specific condition $\eta^{(k)} \ll \|\mathbf{P}\|/(n\|\mathbf{P}\|_\infty)$ therein can be generalized to all finite k 's as long as the initialization $\{y_i^{(0)}\}_{1 \leq i \leq n}$ is concentrated around 0, that is, $\max_{\ell \in [2]} \|\mathbf{y}_\ell^{(0)}\|_\infty^2 \ll \|\mathbf{P}\|/(n\|\mathbf{P}\|_\infty)$. Furthermore, when (α, h) are chosen such that the step-wise deviation diminishes (i.e., $r_n = nh\alpha\|\mathbf{P}\|_\infty + h/n \rightarrow 0$), Proposition 1 indicates that (10) may remain true for even larger numbers of iterations as long as $k = O(r_n^{-1})$.

2.2 Asymptotic Power Iterations, Implicit Spectral Clustering and Early Stopping

With the above graphical interpretation of the updating equation (7) in mind, we now present our key result concerning the asymptotic equivalence between the early exaggeration stage and a power method based on the Laplacian matrix $\mathbf{L}(\alpha\mathbf{P} - \mathbf{H}_n)$. In particular, we make the following assumptions on the initialization and the tuning parameters:

(I2) $\{y_i^{(0)}\}_{1 \leq i \leq n}$ satisfies $\max_{\ell \in [2]} \|\mathbf{y}_\ell^{(0)}\|_\infty^2 = o(\|\mathbf{P}\|/(n\|\mathbf{P}\|_\infty))$ as $n \rightarrow \infty$; and

(T1.D) The parameters (α, h, k) satisfy $\alpha \gg (n\|\mathbf{P}\|)^{-1}$ and $k(nh\alpha\|\mathbf{P}\|_\infty + h/n) = o(1)$ as $n \rightarrow \infty$.

Condition (I2) follows from the discussion subsequent to Proposition 1, which along with Condition (T1.D), which is analogous to but stronger than (T1), ensures the conditions for Theorem 1 and Proposition 1 to hold simultaneously.

Theorem 2 (Asymptotic power iterations). *Under Conditions (I1) (I2) and (T1.D), we have (10) and (12) hold, and so does the asymptotic equivalence*

$$\lim_{n \rightarrow \infty} \frac{\|\mathbf{y}_\ell^{(k)} - [\mathbf{I}_n - h\mathbf{L}(\alpha\mathbf{P} - \mathbf{H}_n)]^k \mathbf{y}_\ell^{(0)}\|_2}{\|\mathbf{y}_\ell^{(0)}\|_2} = 0. \quad (13)$$

The above theorem suggests that each step of the early exaggeration stage may be treated as a power method in the sense that

$$\mathbf{y}_\ell^{(k+1)} \approx [\mathbf{I}_n - h\mathbf{L}(\alpha\mathbf{P} - \mathbf{H}_n)]^k \mathbf{y}_\ell^{(0)}. \quad (14)$$

The normalization by $\|\mathbf{y}_\ell^{(0)}\|_2$ in (13) makes sure the result to be scale-invariant to the initialization. It is well-known that, for a fixed matrix $\mathbf{G} \in \mathbb{R}^{n \times n}$ with 1 as its unique largest eigenvalue in magnitude, the power iteration $\mathbf{y}^{(k)} = \mathbf{G}^k \mathbf{y}^{(0)}$ converges to the associated eigenvector as $k \rightarrow \infty$. As a result, when treated as an approximate power method, the early exaggeration stage of t-SNE essentially aims to find the direction of the leading eigenvector(s) of the matrix $\mathbf{I}_n - h\mathbf{L}(\alpha\mathbf{P} - \mathbf{H}_n)$, which, as will be shown shortly, is actually equivalent to finding the eigenvector(s) associated to the smallest eigenvalue of the Laplacian $\mathbf{L}(\alpha\mathbf{P} - \mathbf{H}_n)$, or the null space of $\mathbf{L}(\mathbf{P})$.

Led by these observations, our next results concern the limiting behavior of the low-dimensional map $\{y_i^{(k)}\}_{1 \leq i \leq n}$ as the number of iterations $k \rightarrow \infty$. Recall that any Laplacian matrix has an eigenvalue 0 associated with a trivial eigenvector $n^{-1/2}\mathbf{1}$. Hence, given the affinity (14) between t-SNE and the power method, we start by showing that, the linear operator $[\mathbf{I}_n - h\mathbf{L}(\alpha\mathbf{P} - \mathbf{H}_n)]^k$ would converge eventually to a projection operator associated to the null space of the Laplacian $\mathbf{L}(\mathbf{P})$. In particular, we let $R \geq 1$ be the dimension of the null space of the Laplacian $\mathbf{L}(\mathbf{P}) \in \mathbb{R}^{n \times n}$; and assume

(T2) the parameters (α, h) satisfies $\kappa < h\lambda_{R+1}(\mathbf{L}(\alpha\mathbf{P})) \leq h\lambda_n(\mathbf{L}(\alpha\mathbf{P})) < 1$ for some constant $\kappa \in (0, 1)$.

This assumption corresponds to the so-called “eigengap” condition in the random matrix literature, which gives the signal strength requirements for the recovery of the eigenvalues/eigenvectors, and, in the meantime, the conditions for the tuning parameters.

Theorem 3 (Convergence of power iterations). *Let $\mathbf{U} \in O(n, R)$ such that its columns consist of an orthogonal basis for the null space of $\mathbf{L}(\mathbf{P})$. Suppose $kh = o(n)$ and (T2) hold. Then, we have*

$$\lim_{k \rightarrow \infty} \frac{\|[\mathbf{I}_n - h\mathbf{L}(\mathbf{P} - \mathbf{H}_n)]^k \mathbf{y} - \mathbf{U}\mathbf{U}^\top \mathbf{y}\|_2}{\|\mathbf{y}\|_2} = 0. \quad (15)$$

Combining Theorems 2 and 3, we know that for sufficiently large n and k , the t-SNE iterations $\mathbf{y}_\ell^{(k)}$ may converge to the projection of the initial vectors $\mathbf{y}_\ell^{(0)}$ into the null space of the Laplacian $\mathbf{L}(\mathbf{P})$, that is

$$\mathbf{y}_\ell^{(k)} \approx \mathbf{U}\mathbf{U}^\top \mathbf{y}_\ell^{(0)}, \quad \ell \in [2]. \quad (16)$$

Now, to better understand the above theorem and its implications on the limiting behavior of t-SNE applied to clustered data, we study the null space of a special class of Laplacian matrices, corresponding to the family of weighted graphs consisting of $R \geq 2$ connected components. In

fact, when the original data $\{X_i\}_{1 \leq i \leq n}$ are well-clustered and τ_i 's are appropriately chosen, the family of disconnected weighted graphs arise naturally since their adjacency matrices are good approximations of \mathbf{P} based on these data (Balakrishnan et al., 2011). We illustrate this point further in Section 4. In the following, we say a symmetric adjacency matrix \mathbf{P} is “well-conditioned” if its associated weighted graph has $R \geq 2$ connected components. Our next result characterizes the Laplacian null space corresponding to these disconnected weighted graphs.

Proposition 2 (Laplacian null space). *Suppose $\mathbf{A} \in \mathbb{R}^{n \times n}$ is symmetric and well conditioned. Then the smallest eigenvalue of the Laplacian $\mathbf{L}(\mathbf{A})$ is 0 and has multiplicity R , and the associated eigen subspace is spanned by $\{\boldsymbol{\theta}_1, \dots, \boldsymbol{\theta}_R\}$ where for each $r \in \{1, \dots, R\}$,*

$$[\boldsymbol{\theta}_r]_j = \begin{cases} 1/\sqrt{n_r} & \text{if the } j\text{-th node belongs to the } r\text{-th component} \\ 0 & \text{otherwise} \end{cases},$$

and n_r is the number of nodes in the r -th connected component. In particular, up to possible permutation of coordinates, any vector \mathbf{u} in the null space of $\mathbf{L}(\mathbf{A})$ can be expressed as

$$\mathbf{u} = \frac{a_1}{\sqrt{n_1}} \begin{bmatrix} \mathbf{1}_{n_1} \\ \mathbf{0} \\ \vdots \\ \mathbf{0} \end{bmatrix} + \frac{a_2}{\sqrt{n_2}} \begin{bmatrix} \mathbf{0} \\ \mathbf{1}_{n_2} \\ \vdots \\ \mathbf{0} \end{bmatrix} + \dots + \frac{a_R}{\sqrt{n_R}} \begin{bmatrix} \mathbf{0} \\ \mathbf{0} \\ \vdots \\ \mathbf{1}_{n_R} \end{bmatrix}, \quad (17)$$

for some $a_1, \dots, a_R \in \mathbb{R}$.

From the above proposition, for a well-conditioned matrix, the components of any \mathbf{u} in the null space of its Laplacian has at most R distinct values, and whenever $|\{a_1, \dots, a_R\}| = R$, the coordinates share the same value if and only if the corresponding nodes fall in the same connected component, i.e., the same cluster.

Building upon the above results, we may generalize our analysis to the cases where \mathbf{P} is only well-conditioned in a weak sense. In other words, we consider instead that there exists a well-conditioned symmetric matrix \mathbf{P}^* sufficiently close to \mathbf{P} , so that the underlying graph associated to \mathbf{P} itself may not be necessarily disconnected. More specifically, we assume

- (T2.D) there exists a symmetric and well-conditioned matrix $\mathbf{P}^* \in \mathbb{R}^{n \times n}$ satisfying
- (T2) and is sufficiently close to \mathbf{P} in the sense that $k\alpha\|\mathbf{L}(\mathbf{P}^* - \mathbf{P})\| = o(1)$.

This condition essentially requires that $\{X_i\}_{1 \leq i \leq n}$ can be well-clustered with proper choices of $\{\tau_i\}$. Again, for given \mathbf{P} satisfying (T2.D), we denote n_r with $r \in [R]$ as the size of the r -th connected component in the graph associated to \mathbf{P}^* . Our next theorem obtains the implicit spectral clustering and early stopping properties of the early exaggeration stage.

Theorem 4 (Implicit clustering and early stopping). *Suppose the similarity \mathbf{P} and the tuning parameters (α, h, k) satisfy (T1.D) and (T2.D), and the initialization satisfies (I1) and (I2). Then there exists some permutation matrix $O \in \mathbb{R}^{n \times n}$ such that, for $\ell \in [2]$,*

$$\lim_{(k,n) \rightarrow \infty} \frac{\|\mathbf{y}_\ell^{(k)} - O\mathbf{z}_\ell\|_2}{\|\mathbf{y}_\ell^{(0)}\|_2} = 0, \quad (18)$$

where

$$\mathbf{z}_\ell = \left(\underbrace{z_{\ell 1}, \dots, z_{\ell 1}}_{n_1}, \underbrace{z_{\ell 2}, \dots, z_{\ell 2}}_{n_2}, \dots, \underbrace{z_{\ell R}, \dots, z_{\ell R}}_{n_R} \right)^\top \in \mathbb{R}^n, \quad (19)$$

and $z_{\ell r} = \boldsymbol{\theta}_r^\top \mathbf{y}_\ell^{(0)} / \sqrt{n_r}$ for $r \in [R]$.

Theorem 4 describes the limiting behavior of the low-dimensional map $\{y_i^{(k)}\}_{1 \leq i \leq n}$ as $(n, k) \rightarrow \infty$, when the original data is properly clustered. Specifically, $\{y_i^{(k)}\}_{1 \leq i \leq n}$ converges cluster-wise towards some limit points on \mathbb{R}^2 , only depending on the initialization, and each associated with a connected component of the underlying graph. It refines and improves the existing results such as Linderman and Steinerberger (2019) and Arora et al. (2018) in various aspects. Firstly, our theoretical framework formalizes and explicates important insights such as the role of the underlying graph Laplacian and the connection to the power method. The theory provides a precise description of the limit points of the low-dimensional map and the theoretical conditions. Secondly, from the perspective of information retrieval theory of dimensionality reduction (Venna et al., 2010; Im et al., 2018; Lui et al., 2018), Theorem 4 suggests that t-SNE achieves asymptotically perfect recall at the end of the early exaggeration stage. This certifies the empirical observation that t-SNE tends to preserve the local structure rather than global structure of the original data (Moon et al., 2019). Lastly, our analysis shows the need of an early stopping of the t-SNE iterations at the early exaggeration stage in order to achieve a better visualization of clustered data. Specifically, both Conditions (T1.D) and (T2.D) allow $k \rightarrow \infty$ but only at a controlled manner. In other words, for each n , there is an (data dependent) upper bound $k(n)$ for k in order for the conditions of Theorem 4 to be satisfied. Such a subtlety is also be observed empirically (Figure 3), where a failure in stopping early would weaken the cluster pattern in $\{y_i^{(k)}\}_{1 \leq i \leq n}$.

2.3 Gradient Flow and Implicit Regularization

For $\ell \in \{1, 2\}$, let $\{\tilde{\mathbf{y}}_\ell^{(k)}\}_{k \geq 0}$ be the sequence defined by the power iterations $\tilde{\mathbf{y}}_\ell^{(k)} = [\mathbf{I}_n - h\mathbf{L}(\alpha\mathbf{P} - \mathbf{H}_n)]^k \mathbf{y}_\ell^{(0)}$. Theorem 2 shows that $\{\tilde{\mathbf{y}}_\ell^{(k)}\}_{k \geq 0}$ well approximates the t-SNE iterations $\{\mathbf{y}_\ell^{(k)}\}_{k \geq 0}$ in the large sample limit. The sequence $\{\tilde{\mathbf{y}}_\ell^{(k)}\}_{k \geq 0}$ admits the updating equation

$$\tilde{\mathbf{y}}_\ell^{(k+1)} = \tilde{\mathbf{y}}_\ell^{(k)} - h\mathbf{L}(\alpha\mathbf{P} - \mathbf{H}_n)\tilde{\mathbf{y}}_\ell^{(k)}, \quad k \geq 0, \quad (20)$$

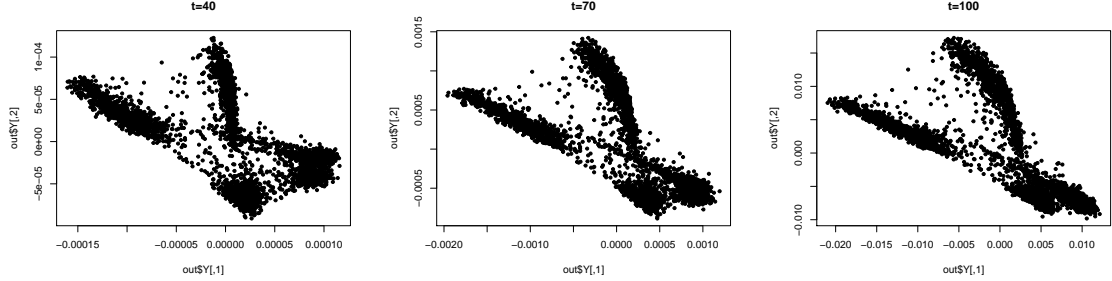


Figure 3: An illustration of the t-SNE iterations at the early exaggeration stage, using the same dataset and the same parameters as in Figure 1, except for without a limit on K_0 . The weakening of the cluster patterns suggests the need of an early stopping.

with an initial value $\tilde{\mathbf{y}}_\ell^{(0)} = \mathbf{y}_\ell^{(0)}$. Treating Equation (20) as an auxiliary gradient descent algorithm to the original algorithm (7), a continuous-time analysis can be developed accordingly, which yields interesting insights about the t-SNE iterations $\{\mathbf{y}_\ell^{(k)}\}_{k \geq 0}$.

We begin by modeling $\{\tilde{\mathbf{y}}_\ell^{(k)}\}_{k \geq 0}$ by a smooth curve $\mathbf{Y}_\ell(t)$ with the Ansatz $\tilde{\mathbf{y}}_\ell^{(k)} \approx \mathbf{Y}_\ell(kh)$. Define a step function $\mathbf{y}_{\ell,h}(t) = \tilde{\mathbf{y}}_\ell^{(k)}$ for $kh \leq t < (k+1)h$, and as $h \rightarrow 0$, $\mathbf{y}_{\ell,h}(t)$ approaches $\mathbf{Y}_\ell(t)$ satisfying

$$\dot{\mathbf{Y}}_\ell(t) = \mathbf{L}(\alpha\mathbf{P} - \mathbf{H}_n)\mathbf{Y}_\ell(t), \quad (21)$$

with the initial value $\mathbf{Y}_\ell(0) = \tilde{\mathbf{y}}_\ell^{(0)} = \mathbf{y}_\ell^{(0)}$. The above first-order differential equation (21) is usually referred as the gradient flow associated with the power iteration sequence $\{\tilde{\mathbf{y}}_\ell^{(k)}\}_{k \geq 0}$, whose limiting behavior can be studied through the step function $\mathbf{y}_{\ell,h}(t)$. The following theorem provides a non-asymptotic uniform upper bound on the deviation of $\mathbf{y}_{\ell,h}(t)$ from $\mathbf{Y}_\ell(t)$ over $t \in [0, T]$ and that of $\tilde{\mathbf{y}}_\ell^{(k)}$ from $\mathbf{Y}_\ell(kh)$ over $k \leq T/h$.

Proposition 3 (Gradient flow). *For $\ell = 1, 2$, and any given $T > 0$, we have*

$$\sup_{t \in [0, T]} \frac{\|\mathbf{y}_{\ell,h}(t) - \mathbf{Y}_\ell(t)\|_2}{\|\mathbf{Y}_\ell(t)\|_2} \leq Th\|\mathbf{L}(\alpha\mathbf{P} - \mathbf{H}_n)\|^2, \quad (22)$$

where $\mathbf{y}_{\ell,h}(t)$ is the continuous-time step process of $\{\tilde{\mathbf{y}}_\ell^{(k)}\}$ generated by (20), and $\mathbf{Y}_\ell(t)$ is the solution to the ordinary differential equation (21). As a consequence, for $t = hk$, if $kh^2\|\mathbf{L}(\alpha\mathbf{P} - \mathbf{H}_n)\|^2 \rightarrow 0$ as $n \rightarrow \infty$, then for $\ell \in \{1, 2\}$,

$$\lim_{(n,k) \rightarrow \infty} \frac{\|\tilde{\mathbf{y}}_\ell^{(k)} - \mathbf{Y}_\ell(hk)\|_2}{\|\mathbf{y}_\ell^{(0)}\|_2} = 0. \quad (23)$$

Combining Theorems 2 and 3, we obtain the approximation $\mathbf{y}_\ell^{(k)} \approx \mathbf{Y}_\ell(kh)$ over a range of $k \geq 0$, for properly chosen parameters (α, h, k) and initialization. Consequently, the properties of

the solution path $\mathbf{Y}_\ell(t)$ may provide important insights on the behavior of the t-SNE algorithm at the early exaggeration stage. We start by stating the following proposition concerning the explicit expression of $\mathbf{Y}_\ell(t)$.

Proposition 4 (Solution path). *For $\ell \in \{1, 2\}$, the first-order linear differential equation (21) with initial value $\mathbf{Y}_\ell(0) = \mathbf{y}_\ell^{(0)}$ has the unique solution $\mathbf{Y}_\ell(t) = \exp(-t\mathbf{L}(\alpha\mathbf{P} - \mathbf{H}_n))\mathbf{y}_\ell^{(0)}$, where $\exp(\cdot)$ is the matrix exponential defined as $\exp(\mathbf{A}) = \sum_{k=0}^{\infty} \frac{1}{k!} \mathbf{A}^k$. In particular, suppose $\mathbf{L}(\mathbf{P})$ have eigendecomposition $\mathbf{L}(\mathbf{P}) = \sum_{i=1}^n \lambda_i \mathbf{u}_i \mathbf{u}_i^\top$ where $0 = \lambda_1 \leq \dots \leq \lambda_n$ and $\mathbf{u}_1 = n^{-1/2} \mathbf{1}_n$. Then we also have*

$$\mathbf{Y}_\ell(t) = (\mathbf{u}_1^\top \mathbf{y}_\ell^{(0)}) \mathbf{u}_1 + \sum_{i=2}^n e^{-t(\alpha\lambda_i - \frac{1}{n-1})} (\mathbf{u}_i^\top \mathbf{y}_\ell^{(0)}) \mathbf{u}_i. \quad (24)$$

Several important observations about the solution path $\mathbf{Y}_\ell(t)$ can be made. Firstly, by Proposition 4, for $\{\mathbf{u}_1, \dots, \mathbf{u}_m\}$ where $m \in [n]$ is the largest integer such that $\alpha\lambda_m \leq \frac{1}{n-1}$, we have

$$\lim_{t \rightarrow \infty} \mathbf{Y}_\ell(t) \in \text{span}(\{\mathbf{u}_1, \dots, \mathbf{u}_m\}). \quad (25)$$

This can be treated as a continuous version of the limiting behavior of the power iterations obtained in Theorem 3: under the conditions of Theorem 3, we have $\alpha\lambda_m \leq \frac{1}{n-1}$ for all $m \in [R]$ but $\alpha\lambda_{R+1} > \frac{1}{n-1}$, so that (25) implies that $\mathbf{Y}_\ell(t)$ converges to the null space of $\mathbf{L}(\mathbf{P})$. Secondly, as long as $t = O(n)$, by orthogonality of $\{\mathbf{u}_i\}$, we have

$$\|\mathbf{Y}_\ell(t)\|_2^2 \leq C \sum_{i=1}^n e^{-2t\alpha\lambda_i} (\mathbf{u}_i^\top \mathbf{y}_\ell^{(0)})^2, \quad (26)$$

for some absolute constant $C > 0$. The right-hand side is monotonically nonincreasing in t . Hence, the average distance of the rows in $(\mathbf{Y}_1(hk), \mathbf{Y}_2(hk))$ to the origin remains non-expansive over the iterations and is bounded up to a constant by that of $(\mathbf{Y}_1(0), \mathbf{Y}_2(0))$. This result echos Proposition 1 based on the discrete-time analysis.

The third and more insightful observation from (24) is its implications on the finite-time behavior of the original t-SNE sequence $\{\mathbf{y}_\ell^{(k)}\}_{k \geq 1}$, which complements our discrete-time analysis. Specifically, for finite $t > 0$, the coefficient of the i -th basis \mathbf{u}_i in $\mathbf{Y}_\ell(t)$ is proportional to $e^{-t\alpha\lambda_i}$, which is nonincreasing in λ_i . Consequently, (24) implies that, in the early steps of the iterations, the t-SNE algorithm imposes an implicit regularization effect on the low-dimensional data points $\{y_i^{(k)}\}_{1 \leq i \leq n}$, in the sense that

$$\mathbf{y}_\ell^{(k)} \approx n^{-1} (\mathbf{1}_n^\top \mathbf{y}_\ell^{(0)}) \mathbf{1}_n + \sum_{i=2}^n e^{-kh(\alpha\lambda_i - \frac{1}{n-1})} (\mathbf{u}_i^\top \mathbf{y}_\ell^{(0)}) \mathbf{u}_i. \quad (27)$$

Comparing to the limit (25) or (16), during the early steps of the iterations, $\mathbf{y}_\ell^{(k)}$ is regularized as a conical sum of all the eigenvector basis $\{\mathbf{u}_i\}_{1 \leq i \leq n}$, with larger weights on the eigenvectors

\mathbf{u}_i corresponding to the smaller eigenvalues of $\mathbf{L}(\mathbf{P})$, and smaller weights on those corresponding to the larger eigenvalues of $\mathbf{L}(\mathbf{P})$. As the iteration step increases, the contributions from the less informative eigenvectors with larger eigenvalues λ_i such that $\alpha\lambda_i > \frac{1}{n-1}$ decrease exponentially in t , whereas the contributions from the more informative eigenvectors with smaller eigenvalues λ_i such that $\alpha\lambda_i < \frac{1}{n-1}$ increase with t .

Importantly, the inclusion of all the eigenvectors helps t-SNE to better summarize the cluster information in the original data and avoid convergence to the trivial eigenvector $n^{-1/2}\mathbf{1}_n$. Indeed, the convergence (25) by itself may not lead to a cluster structure in the limit, as in many applications the graph corresponding to \mathbf{P} may be simply connected under finite samples, so that the null space is effectively spanned by $n^{-1/2}\mathbf{1}$ alone. However, as our next theorem shows, the benefit of the implicit regularization, brought about by stopping early at the exaggeration stage, can be seen in the creation of desirable clusters embodied in the underlying true graph corresponding to a well-conditioned \mathbf{P}^* . In particular, we make the following assumptions analogous to (T1.D) and (T2.D) in the discrete-time analysis.

(T1.C) the parameters (α, h, t) satisfy $\alpha \gg [n\lambda_{R+1}(\mathbf{L}(\mathbf{P}))]^{-1}$ and $t = o(n)$ as $n \rightarrow \infty$;

(T2.C) there exists a symmetric and well-conditioned matrix $\mathbf{P}^* \in \mathbb{R}^{n \times n}$ such that $\lambda_{R+1}(\mathbf{L}(\mathbf{P}^*)) \gg \max\{(t\alpha)^{-1}, \|\mathbf{L}(\mathbf{P}^* - \mathbf{P})\|\}$, and $t\alpha\|\mathbf{L}(\mathbf{P}^* - \mathbf{P})\| = o(1)$ as $n \rightarrow \infty$.

Similar to the previous results, Condition (T1.C) concerns the lower bound for the exaggeration parameter α , and an upper bound for the cumulative deviation, whereas Condition (T2.C) ensures the eigengap condition and the closeness between \mathbf{P}^* and \mathbf{P} .

Theorem 5 (Implicit regularization, clustering and early stopping). *Under Conditions (I1), (T1.C) and (T2.C), let $\mathbf{U}_0 \in O(n, R)$ such that its columns span the null space of \mathbf{P}^* . Then, we have*

$$\lim_{n \rightarrow \infty} \frac{\|\mathbf{Y}_\ell(t) - \mathbf{U}_0 \mathbf{U}_0^\top \mathbf{Y}_\ell(t)\|_2}{\|\mathbf{Y}_\ell(0)\|_2} = 0, \quad \ell \in \{1, 2\}, \quad (28)$$

and, for \mathbf{z}_ℓ defined in Theorem 4, there exists a permutation matrix $O \in \mathbb{R}^{n \times n}$ such that

$$\lim_{n \rightarrow \infty} \frac{\|\mathbf{Y}_\ell(t) - O\mathbf{z}_\ell\|_2}{\|\mathbf{Y}_\ell(0)\|_2} = 0, \quad \ell \in \{1, 2\}. \quad (29)$$

An immediate consequence of the above theorem is the following corollary, which arrives at the same conclusion as Theorem 4 through a different route.

Corollary 1. *Suppose the conditions of Theorems 2 and 5 hold with $t = hk$, and $k\alpha^2h^2\|\mathbf{L}(\mathbf{P} - \mathbf{H}_n)\|^2 \rightarrow 0$. Then the conclusion of Theorem 4 holds.*

The above theorems provide a theoretical explanation of the need of early stopping at the early exaggeration stage. On the one hand, the number of iterations should be sufficiently large so that

$\{y_i^{(k)}\}_{1 \leq i \leq n}$ moves away from the initialization and is sufficiently close to a subspace where the underlying cluster information is properly stored. On the other hand, the iterations should be also stopped early (not exceeding a certain bound) to avoid “over-fitting,” that is, convergence to the null space of the superficial Laplacian $\mathbf{L}(\mathbf{P})$, which may only include the non-informative trivial eigenvector $n^{-1/2}\mathbf{1}_n$.

3 Theoretical Analysis of the Embedding Stage

We have shown in Section 2 that the iterations in the early exaggeration stage essentially create clusters in the low-dimensional map $\{y_i^{(k)}\}_{1 \leq i \leq n}$, that agree with those underlying $\{X_i\}_{1 \leq i \leq n}$. However, as indicated by Proposition 1, so far the low-dimensional map is concentrated and localized around zero, which may not be ideal for visualization purpose. In addition, by Theorem 4, much information about $\{X_i\}_{1 \leq i \leq n}$ other than its cluster membership are not reflected by the low-dimensional map. In this section, we show that, after transition to the embedding stage, the t-SNE iterations (5) essentially start by amplifying and refining the existing cluster structures in the low-dimensional map and then aim at a proper embedding of the original data.

Starting from the embedding stage, the diameter of the low-dimensional map $\{y_i^{(k)}\}_{1 \leq i \leq n}$ grows fast and they move in clusters as inherited from the early exaggeration stage. Importantly, over the iterations, the elements of $\{y_i^{(k)}\}_{1 \leq i \leq n}$ belonging to different clusters would in general move away from each other, resulting to an enlarged visualization with more separated clusters. We refer these iteration steps presenting such an expansive, and intercluster-repulsive behavior of $\{y_i^{(k)}\}_{1 \leq i \leq n}$ as the amplification phase of the embedding stage. Theoretically, we show that this phase can be characterized by the boundedness of $\text{diam}(\{y_i^{(k)}\}_{1 \leq i \leq n})$. That is, the amplification stops whenever $\text{diam}(\{y_i^{(k)}\}_{1 \leq i \leq n})$ exceeds a certain constant threshold.

Recall that the updating equation at the embedding stage is

$$y_i^{(k+1)} = y_i^{(k)} + h' \sum_{j \neq i} S_{ij}^{(k)} (y_j^{(k)} - y_i^{(k)}), \quad (30)$$

where h' is the step size that may not be identical to the one in the early exaggeration stage. To understand the behavior of t-SNE at this stage, we start with the following proposition characterizing the matrix $\mathbf{S}^{(k)} = (S_{ij}^{(k)})_{1 \leq i, j \leq n}$ over the amplification phase.

Proposition 5. *For any integer k , if $\text{diam}(\{y_i^{(k)}\}_{1 \leq i \leq n}) = o(1)$ as $n \rightarrow \infty$, then, for any $i, j \in [n]$ such that $i \neq j$,*

1. *if $\lim_{n \rightarrow \infty} n^2 p_{ij} = 0$, it holds that $S_{ij}^{(k)} = -\frac{1+O(\eta^{(k)})}{n(n-1)}$ as $n \rightarrow \infty$; and*
2. *if $\lim_{n \rightarrow \infty} n^2 p_{ij} \geq c$ for some constant $c > 0$, it holds that $|S_{ij}^{(k)}| \asymp p_{ij}$ as $n \rightarrow \infty$.*

Roughly speaking, Proposition 5 says that over the amplification phase, the matrix $\mathbf{S}^{(k)} = (S_{ij}^{(k)})_{1 \leq i, j \leq n}$ essentially has two types of entries, determined by the magnitude of the corresponding entries in \mathbf{P} . Specifically, $S_{ij}^{(k)}$ is negative with magnitude n^{-2} if p_{ij} is much smaller than n^{-2} , and otherwise $S_{ij}^{(k)}$ has the same magnitude as p_{ij} . This observation leads to the next theorem, which provides important insights on the updating equation (30) by partitioning the contributions of $\{y_i^{(k)}\}_{1 \leq i \leq n}$ to an updated $y_i^{(k+1)}$ into a few major components, each corresponding to a distinct cluster in the original data. To this end, we consider again the similarity matrix \mathbf{P} that is well-conditioned in the weak sense, characterized by the following assumption.

(T2.E) There exists a symmetric and well-conditioned matrix $\mathbf{P}^* \in \mathbb{R}^{n \times n}$ satisfying

(T2.D), $\lim_{n \rightarrow \infty} n^2 \|\mathbf{P} - \mathbf{P}^*\|_\infty = 0$, and $\lim_{n \rightarrow \infty} \frac{n_r}{n} \rightarrow \gamma_r \in (0, 1)$ for each $r \in [R]$.

The existence of well-conditioned \mathbf{P}^* induces an equivalence class on $[n]$ characterizing the underlying cluster membership. Specifically, for any $i, j \in [n]$, we denote $i \sim j$ if and only if the i -th node and the j -th node belong to the same graph component. Therefore, we have the partition $[n] = \cup_{r \in [R]} H_r$ for mutually disjoint sets $\{H_r\}_{1 \leq r \leq R}$, with H_r corresponding to the r -th equivalence class.

Next, we make assumptions on the initialization and parameters (α, h, K_0) in early exaggeration stage, where $K_0 = K_0(n) \rightarrow \infty$ is the total number of iterations in that stage. Specifically, we assume

(I3) the initialization is chosen such that $\|\mathbf{y}_1^{(0)}\|_2 \asymp \|\mathbf{y}_2^{(0)}\|_2$, $\max_{\ell \in [2]} \|\mathbf{y}_\ell^{(0)}\|_\infty = o(n^{-1/2})$ as $n \rightarrow \infty$, and there exists some constant $C > 1$ such that \mathbf{z}_ℓ defined in Theorem 4 satisfies $C^{-1} \leq n|z_{\ell i} - z_{\ell j}|/\|\mathbf{y}_\ell^{(0)}\|_2 \leq C$ for any $i, j \in [R]$ such that $i \neq j$, and $\ell \in \{1, 2\}$;

(T1.E) the parameters (α, h, K_0) in (6) satisfy (T1.D), and, for $R_n = (1 - \kappa)^{K_0} + hK_0[(\alpha n \|\mathbf{P}\|_\infty + 1/n) \cdot \max_{\ell \in [2]} \|\mathbf{y}_\ell^{(0)}\|_\infty^2 + \alpha \|\mathbf{L}(\mathbf{P}^* - \mathbf{P})\|]$, we have $nR_n(1 + n^2 \|\mathbf{P}^*\|_\infty) = o(1)$ as $n \rightarrow \infty$.

Condition (I3) is mild as it can be satisfied with high probability by a straightforward random initialization procedure, to be presented shortly. Condition (T1.E) is analogous to but stronger than (T1.D), by requiring a smaller cumulative approximation error R_n , between $\mathbf{L}(\mathbf{S}_\alpha^{(k)})$ and $\mathbf{L}(\alpha \mathbf{P}^* - \mathbf{H}_n)$. It essentially requires more distinct clusters in $\{X_i\}_{1 \leq i \leq n}$.

Finally, for the parameters (h', K_1) in embedding stage, where $K_1 = K_1(n)$ is the number of iterations within the amplification phase, we make the following assumption that controls the cumulative approximation error in $\mathbf{S}^{(k)}$ as suggested by Proposition 5.

(T3.E) $\text{diam}(\{y_i^{(K_0+K_1)}\}_{1 \leq i \leq n}) = o(1)$, and the parameter h' in (30) satisfies $K_1 h' (n \|\mathbf{P}^*\|_\infty + 1/n) = O(1)$ as $n \rightarrow \infty$.

Theorem 6 (Intercluster repulsion). *Under Conditions (T1.E) (T2.E) (T3.E) and (I3), for each $K_0 \leq k \leq K_0 + K_1$ and any $i \in [n]$, we have*

$$y_i^{(k+1)} = y_i^{(k)} + \sum_{r \in [R] \setminus r_0} f_{ir}^{(k)} + \epsilon_i^{(k)}, \quad (31)$$

where $r_0 \in [R]$ such that $i \in H_{r_0}$, $\lim_{n \rightarrow \infty} \|\epsilon_i^{(k)}\|_2 / \|f_{ir}^{(k)}\|_2 = 0$ for all $r \in [R] \setminus r_0$, and

$$f_{ir}^{(k)} = \frac{h'|H_r|}{n(n-1)} \left(y_i^{(k)} - \frac{1}{|H_r|} \sum_{j \in H_r} y_j^{(k)} \right) \in \mathbb{R}^2.$$

In addition, we have

$$\sup_{K_0 \leq k \leq K_0 + K_1} \max_{(i,j):i \sim j} \|y_i^{(k)} - y_j^{(k)}\|_2 \ll n^{-1} (\|\mathbf{y}_1^{(0)}\|_2 + \|\mathbf{y}_2^{(0)}\|_2), \quad (32)$$

and

$$\inf_{K_0 \leq k \leq K_0 + K_1} \min_{(i,j):i \sim j} \|y_i^{(k)} - y_j^{(k)}\|_2 \gtrsim n^{-1} (\|\mathbf{y}_1^{(0)}\|_2 + \|\mathbf{y}_2^{(0)}\|_2). \quad (33)$$

A few remarks about the above theorem are in order. Firstly, Conditions (T1.E) (T2.E) and (I3) concerning the initialization, parameter selection and the number of iterations in the early exaggerations are not only compatible but also sufficient for the previous results, including Theorems 2 and 4. This suggests the above intercluster repulsive phenomenon at the embedding stage actually relies on the properties of the outputs from the early exaggeration stage, again yielding the necessity of such an early exaggeration technique. Secondly, as indicated by the next theorem, Condition (I3) on the initialization can be satisfied by the following simple local random initialization procedure.

Theorem 7 (Random initialization). *For any sequence $\sigma_n \rightarrow 0$ as $n \rightarrow \infty$, let $\mathbf{y}_\ell^{(0)} = \sigma_n \mathbf{g}_\ell / \|\mathbf{g}_\ell\|_2$, where $\mathbf{g}_\ell \in \mathbb{R}^n$ for $\ell \in [2]$ is independently generated from a standard multivariate normal distribution. Then $\{y_i^{(0)}\}_{1 \leq i \leq n}$ satisfies Condition (I3) with probability at least $1 - \delta$ for some sufficiently small constant $\delta > 0$.*

Thirdly, the above theorem provides a precise characterization of the kinematics of each y_i^k during the iterations, and its reliance on the data points $\{y_i^{(k-1)}\}$ in the previous step, as well as the cluster structure inherited from the early exaggeration stage. Specifically, $f_{ir}^{(k)}$ summarizes the contributions from the points $\{y_i^{(k)}\}_{i \in H_r}$ in the r -th cluster to the new point $y_i^{(k+1)}$. The theorem implies that, at the amplification phase, the behavior of $\{y_i^{(k)}\}_{1 \leq i \leq n}$ is mainly driven by the relative positions of the R clusters produced in the early exaggeration stage: for each point, a vector sum of the *repulsive forces* coming from all the other clusters at their current positions determine the direction and distance of its movement of each point in this iteration (Figure 2). As a consequence,

after each iteration, the diameter of $\{y_i^{(k)}\}_{1 \leq i \leq n}$ would increase, till the end of the amplification phase, that is, when Condition (T3.E), or more specifically, $\text{diam}(\{y_i^{(k)}\}_{1 \leq i \leq n}) = o(1)$ no longer holds. This process improves the visualization quality by making the clusters more distinct and separated (Figure 1 with $k = 40$ and 80).

Our next result confirms the intuition that the diameter of $\{y_i^{(k)}\}_{1 \leq i \leq n}$ is bound to increase after each iteration in the amplification phase of the embedding stage.

Theorem 8 (Expansion). *Suppose the conditions of Theorem 6 hold. If in addition $\|\mathbf{P}^*\|_\infty \lesssim n^{-2}$, then for any $k \in \{K_0, K_0 + 1, \dots, K_1\}$, we have*

$$\text{diam}(\{y_i^{(k+1)}\}_{1 \leq i \leq n}) > \text{diam}(\{y_i^{(k)}\}_{1 \leq i \leq n}), \quad (34)$$

where $\text{diam}(\{y_i^{(k+1)}\}_{1 \leq i \leq n}) - \text{diam}(\{y_i^{(k)}\}_{1 \leq i \leq n}) \gtrsim \frac{h'}{n^2} \min_{\ell=1,2} \|\mathbf{y}_\ell^{(0)}\|_2$.

Once the diameter of $\{y_i^{(k)}\}_{1 \leq i \leq n}$ exceeds certain threshold, that is, when $\text{diam}(\{y_i^{(k)}\}_{1 \leq i \leq n})$ is at least of constant order, we arrive at the final stabilization phase. In this phase, the condition of Proposition 5 is violated, and, unlike what is claimed in part one of Proposition 5, the entries of the matrix $\mathbf{S}^{(k)}$ corresponding to the smaller entries in \mathbf{P} , that is, p_{ij} 's with $p_{ij} \ll n^{-2}$, no longer remain an almost constant value $1/n(n-1)$. In particular, the sign of $S_{ij}^{(k)}$ would generally rely on the relative magnitudes between p_{ij} and q_{ij} .

We rewrite (30) as

$$y_i^{(k+1)} = y_i^{(k)} + h' \sum_{j \neq i} \frac{p_{ij} - q_{ij}^{(k)}}{1 + d_{ij}^{(k)}} (y_j^{(k)} - y_i^{(k)}). \quad (35)$$

In the stabilization phase, the new position for $y_i^{(k+1)}$ is determined by starting from $y_i^{(k)}$, and averaging the contributions from each of the other data points $\{y_j^{(k)}\}_{j \neq i}$. The contribution from $y_j^{(k)}$ to $y_i^{(k+1)}$ is either in or against the direction of $(y_j^{(k)} - y_i^{(k)})$, depending on $\text{sign}(p_{ij} - q_{ij})$. If $\text{sign}(p_{ij} - q_{ij}) = 1$, or, the distance between $y_i^{(k)}$ and $y_j^{(k)}$ as measured by q_{ij} is smaller than the distance between X_i and X_j as measured by p_{ij} , the contribution from $y_j^{(k)}$ to $y_i^{(k+1)}$ is in the direction of $y_j^{(k)} - y_i^{(k)}$, resulting to a repulsive force that enlarges the distance between $y_i^{(k+1)}$ and $y_j^{(k+1)}$ after the iteration. Similarly, if $\text{sign}(p_{ij} - q_{ij}) = -1$, it means the distance between $y_i^{(k)}$ and $y_j^{(k)}$ is larger than their counterparts in $\{X_i\}_{1 \leq i \leq n}$, so the contribution $y_j^{(k)}$ to $y_i^{(k+1)}$ is in the opposite direction $y_j^{(k)} - y_i^{(k)}$, resulting to an attractive force that reduces the distance between $y_i^{(k+1)}$ and $y_j^{(k+1)}$ after the iteration. The iterations over the stabilization phase aim to locally adjust the relative positions of the low-dimensional map to make them a more reliable representation or embedding of the high-dimensional data points.

4 Applications: Visualizing Model-Based Clustered Data

In the previous sections, we established the theoretical properties for the basic t-SNE algorithm under general conditions on the parameters $(\alpha, h, h', K_1, K_2)$, the initialization, and the similarity matrix \mathbf{P} constructed from the original data. In this section, we demonstrate the implications of these general conditions in various applications, by applying our theory in two concrete settings of clustered data, one generated from a Gaussian mixture model and another from a noisy nested sphere model.

4.1 Gaussian Mixture Model

Consider the Gaussian mixture model

$$X_i|z_i = r \sim N(\mu_r, \Sigma), \quad z_i \stackrel{i.i.d.}{\sim} \text{Multinomial}(\pi_1, \dots, \pi_R), \quad \text{for } i \in [n], \quad (36)$$

where $\mu_r \in \mathbb{R}^p$ and $\sum_{r=1}^R \pi_r = 1$. We make the following assumptions.

- (C1) The mixing proportions $\{\pi_r\}_{1 \leq r \leq R}$ satisfy $\min_r \pi_r \geq c > 0$.
- (C2) There exists some large constant $C' > 0$ such that $\rho^2 = \min_{1 \leq j \neq k \leq R} \|\mu_j - \mu_k\|_2^2 \geq C' \max\{p, \log n\}$.
- (C3) There exists some constant $C > 0$ such that the population covariance matrix $\Sigma \in \mathbb{R}^{p \times p}$ satisfies $C^{-1} \leq \lambda_1(\Sigma) \leq \lambda_p(\Sigma) \leq C$ and $\text{tr}(\Sigma)/p \leq C$.

Based on the above Gaussian mixture model, we obtain the following corollary that provides the conditions for the theoretical properties presented in the previous sections. The result implies the range of appropriate tuning parameters for visualizing the model-generated data with t-SNE.

Corollary 2. *Suppose Conditions (C1) (C2) and (C3) hold, and $\tau_i^2 \asymp \max\{p, \log n\}$. If $\alpha \gg 1$, $K_0 h = o(n)$, $h\alpha \asymp n$, $1 \ll K_0 \ll \exp\{\frac{\rho^2}{\max\{p, \log n\}}\}$ and $K_0 h\alpha \sigma_n^2 \log n = o(n^2)$, then Conditions (T1.D) and (T2.D) hold. If in addition $\log n \ll K_0 \ll n^{-1} \exp\{\frac{\rho^2}{\max\{p, \log n\}}\}$, $K_0 h\alpha \sigma_n^2 \log n = o(n)$, and $K_1 h' = O(n)$, then Conditions (T1.E) (T2.E) and (T3.E) hold.*

As a consequence, suitable choices of the tuning parameters $(\alpha, h, h', K_0, K_1)$ under the Gaussian mixture model can be determined efficiently. For example, if $\rho^2 \gtrsim \log n \cdot \max\{p, \log n\}$, one could choose $K_0 = \log^2 n$, $\sigma_n = (\log n)^{-2}$, $h = h' = n^\delta$ and $\alpha = n^{1-\delta}$ for any constant $\delta \in (0, 1)$. By Corollary 2, Conditions (T1.D) and (T2.D) hold, so the conclusions of Theorem 4 follows for $k = K_0$; meanwhile, Conditions (T1.E) (T2.E) and (T3.E) also hold, so the conclusions of Theorem 6 hold for each K_1 with $K_0 \leq K_1 \leq n^{1-\delta}$. Note that the above results apply to both low-dimensional settings where $p = o(n)$ and high-dimensional settings where $p \gtrsim n$. The bandwidths $\{\tau_i\}_{1 \leq i \leq n}$ take the same value that only depends on the sample size and dimensionality of the original data.

4.2 Noisy Nested Sphere Model

Consider the model of nested spheres with radial noise (Amini and Razaee, 2019), where for $i \in [n]$, we have

$$X_i = \mu_i + \frac{\mu_i}{\|\mu_i\|_2} \xi_i, \quad \xi_i \stackrel{i.i.d.}{\sim} N(0, \sigma^2) \quad (37)$$

and

$$\mu_i | z_i = r \sim P_k, \quad z_i \stackrel{i.i.d.}{\sim} \text{Multinomial}(\pi_1, \dots, \pi_R), \quad (38)$$

with $\sum_{r=1}^R \pi_r = 1$ and $\{P_k\}$ being uniform distributions on nested spheres in \mathbb{R}^p of various radii $\rho_{\min} = \rho_1 < \rho_2 < \dots < \rho_R = \rho_{\max}$. We make the following assumptions concerning the separation distances between the underlying nested spheres.

(C4) There exists some γ such that $\max\{n^{-1}, \sigma^2 \rho_{\min}^{-2}\} \log n \ll \gamma \ll 1$ and $\max_{r \in [R-1]} \frac{\rho_r}{\rho_{r+1}} \ll 1 - C\sqrt{\gamma \log \gamma}$ for some sufficiently large constant $C > 0$.

(C5) There exists some small constant $c > 0$ such that $c \min |\rho_{r+1} - \rho_r| \geq \sigma \sqrt{\log n}$.

In Condition (C4), the separation distance is characterized by the ratio ρ_r / ρ_{r+1} whereas in Condition (C5) the distance is characterized by the difference $\rho_{r+1} - \rho_r$. The following corollary provides a sufficient condition for the results presented in the previous sections under the noisy nested sphere model.

Corollary 3. *Suppose Assumptions (C1) (C4) and (C5) hold, and $\tau_i^2 \asymp \gamma \rho_{z_i}^2$. If $K_0 h = o(n)$, $\alpha h = O(\gamma n)$, $h \alpha \lambda_{R+1}(\mathbf{L}(\mathbf{P}^*)) \geq \kappa$ for some constant $\kappa \in (0, 1)$, $K_0 \gg 1$, $K_0 h(\alpha/\gamma + 1) \sigma_n^2 \log n = o(n^2)$, and $\log \frac{K_0 h \alpha}{n} \ll \gamma^{-1} (1 - \max_{r \in [R-1]} \frac{\rho_r}{\rho_{r+1}})^2 + \log \gamma$, then Conditions (T1.D) and (T2.D) hold. If in addition $K_0 \gg \log n$, $K_0 h(\alpha/\gamma + 1) \sigma_n^2 \log n = o(n)$, $\log K_0 h \alpha \ll \gamma^{-1} (1 - \max_{r \in [R-1]} \frac{\rho_r}{\rho_{r+1}})^2 + \log \gamma$, and $K_1 h' = O(\gamma n)$, then Conditions (T1.E) (T2.E) and (T3.E) hold.*

Again, suitable choices of the tuning parameters $(\alpha, h, h', K_0, K_1)$ under the noisy nested sphere model can be determined efficiently. For example, let's consider the case where $\rho_{r+1} - \rho_r = \Delta$ for all $r \in [R-1]$. Specifically, suppose there exists some small constant $c > 0$ such that $\Delta \geq c \rho_R$, and that $\gamma = c(\log n)^{-1}$ satisfies (C4) and $\lambda_{R+1}(\mathbf{L}(\mathbf{P}^*)) \gtrsim \frac{1}{\gamma n}$ in probability. Then, by Corollary 3, the desired visualization properties such as those in Theorems 4 and 6 would hold with high probability, as long as we choose $K_0 = \log^2 n$, $K_1 \leq n^{1-\delta} / \log n$, $\sigma_n = (\log n)^{-2}$, $h = h' = n^\delta$ and $\alpha = \gamma n^{1-\delta}$ for any constant $\delta \in (0, 1)$.

5 Discussion

The present paper provides theoretical foundations of t-SNE for visualizing clustered data and obtains many insights about its theoretical properties and interpretations. However, there are still many interesting questions that remain unexplored. For instance, what is the limiting behavior

of the low-dimensional map $\{y_i^{(k)}\}_{1 \leq i \leq n}$ towards the end of the embedding stage, after transition to the stabilization phase? How many iterations are needed for the embedding stage? How to determine the bandwidth $\{\tau_i\}$ in a data-driven and adaptive manner? The present work is a first step towards answering these important questions.

Moreover, our theoretical framework is generic and can be generalized to study other algorithms that are closely related to or share similar features with t-SNE. For example, in addition to the variants of t-SNE mentioned in Section 1, many dimension reduction and data visualization methods, such as multidimensional scaling (Kruskal, 1978), kernel principal component analysis (Schölkopf et al., 1997), and Laplacian eigenmap (Belkin and Niyogi, 2003), start with a similarity matrix summarizing the pairwise distances within a dataset, and then proceed by either explicitly or implicitly exploiting the spectral properties of the similarity matrix. In this connection, the general ideas behind our theoretical analysis, such as identifying the underlying structured graph and properties of its adjacency or Laplacian matrix (Sections 2.1 and 2.2), studying the gradient flow associated with the discrete algorithm (Section 2.3), and the mechanical/kinematic view of the updating equation (Section 3), can be adopted to uncover the underlying mechanism and the properties of these methods.

It is also interesting to explore the fundamental limit for data visualization and dimension reduction. For example, what are the necessary conditions for the data set $\{X_i\}_{1 \leq i \leq n}$ to guarantee the existence of a low-dimensional map $\{y_i\}_{1 \leq i \leq n}$ being a metric embedding of it? Whether t-SNE has to sacrifice some global structures in order to locally embed the data well? These problems are left for future investigation.

6 Proofs of Some Main Results

In this part, we present our proofs of the main theorems in Sections 2.1 and 2.2, including Theorems 1, 2, 3 and 4, and Propositions 1 and 2. The space reason, the proofs of other theorems are collected in Appendix.

6.1 Proof of Theorem 1

For simplicity, we ignore the superscript (k) in $y_i^{(k)}, q_{ij}^{(k)}, \eta^{(k)}$ and $S_{ij}^{(k)}(\alpha)$. Since $S_{ij}(\alpha) = \frac{\alpha p_{ij} - q_{ij}}{1 + \|y_i - y_j\|_2^2}$, if we denote $d_{ij} = \|y_i - y_j\|_2^2$, we have

$$\begin{aligned} \left| S_{ij}(\alpha) - \alpha p_{ij} + \frac{1}{n(n-1)} \right| &\leq \left| \alpha p_{ij} - \frac{\alpha p_{ij}}{1 + d_{ij}} \right| + \left| \frac{q_{ij}}{1 + d_{ij}} - \frac{1}{n(n-1)} \right| \\ &= d_{ij} \alpha p_{ij} + \left| \frac{1}{Z(1 + d_{ij})^2} - \frac{1}{n(n-1)} \right|, \end{aligned}$$

where

$$Z = \sum_{i \neq j} (1 + d_{ij})^{-1} = \sum_{i \neq j} \left(1 - \frac{d_{ij}}{1 + d_{ij}} \right) = n(n-1) - \sum_{i \neq j} \frac{d_{ij}}{1 + d_{ij}} \equiv n(n-1) - \Delta.$$

Now since $\Delta \leq n(n-1) \min\{\eta, 1\} = n(n-1)\eta$, we have

$$\begin{aligned} \left| \frac{1}{Z(1 + d_{ij})^2} - \frac{1}{n(n-1)} \right| &= \left| \frac{(1 + d_{ij})^{-2}n(n-1) - n(n-1) + \Delta}{n^2(n-1)^2 - n(n-1)\Delta} \right| \\ &\leq \frac{|[(1 + d_{ij})^{-2} - 1]n(n-1) + \Delta|}{n^2(n-1)^2(1-\eta)} \leq \frac{2\eta}{n(n-1)(1-\eta)} \end{aligned} \quad (39)$$

Hence

$$\left| S_{ij}(\alpha) - \alpha p_{ij} + \frac{1}{n(n-1)} \right| \leq \eta \alpha p_{ij} + \frac{2\eta}{n(n-1)(1-\eta)}.$$

For the second statement, we note that

$$\|\mathbf{H}_n\| \leq \frac{1}{n-1} + \frac{1}{n(n-1)} \lesssim \frac{1}{n}. \quad (40)$$

Then as long as $\|\alpha\mathbf{P}\| \gg \frac{1}{n}$, we have $\|\alpha\mathbf{P} - \mathbf{H}_n\| \geq \|\alpha\mathbf{P}\| - \frac{1}{n} \asymp \|\alpha\mathbf{P}\|$. Therefore, under the condition that $\eta \ll \frac{\|\mathbf{P}\|}{n\|\mathbf{P}\|_\infty} \leq 1$,

$$\frac{\|\mathbf{S}_\alpha - (\alpha\mathbf{P} - \mathbf{H}_n)\|}{\|\alpha\mathbf{P} - \mathbf{H}_n\|} \lesssim \frac{n\|\mathbf{S}_\alpha - (\alpha\mathbf{P} - \mathbf{H}_n)\|_\infty}{\|\alpha\mathbf{P}\|} \lesssim \frac{\alpha n\|\mathbf{P}\|_\infty\eta + \eta/n}{\|\alpha\mathbf{P}\|}$$

Then, the first term $\eta n\|\mathbf{P}\|_\infty/\|\mathbf{P}\| \rightarrow 0$ as $\eta \ll \|\mathbf{P}\|/(n\|\mathbf{P}\|_\infty)$; the second term $\frac{\eta}{n\alpha\|\mathbf{P}\|} \lesssim \frac{1}{n\alpha\|\mathbf{P}\|} \rightarrow 0$ as $\alpha \gg (n\|\mathbf{P}\|)^{-1}$.

6.2 Proof of Proposition 1

Note that for any $k \geq 0$,

$$y_{\ell i}^{(k+1)} \leq \|[\mathbf{I} - h\mathbf{L}(\mathbf{S}_\alpha^{(k)})]_{i.}\|_1 \|\mathbf{y}_\ell^{(k)}\|_\infty,$$

where

$$\|[\mathbf{I} - h\mathbf{L}(\mathbf{S}_\alpha^{(k)})]_{i.}\|_1 = \left| 1 - h \sum_{j=1}^n S_{ij}^{(k)}(\alpha) \right| + h \sum_{j \neq i} |S_{ij}^{(k)}(\alpha)| \leq 1 + 2h \left| \sum_{j=1}^n S_{ij}^{(k)}(\alpha) \right|.$$

For the last term, we have

$$h \sum_{j=1}^n |S_{ij}^{(k)}(\alpha)| \leq hn\|\mathbf{S}_\alpha^{(k)}\|_\infty \leq nh(\alpha\|\mathbf{P}\|_\infty + \|\mathbf{Q}^{(k)}\|_\infty) \leq nh\alpha\|\mathbf{P}\|_\infty + \frac{h(1 + \eta^{(k)})}{n}$$

where the last inequality follows from (39). Then we have $y_{\ell i}^{(k+1)} \leq (1+2nh\alpha\|\mathbf{P}\|_\infty + \frac{h(1+\eta^{(k)})}{n})\|\mathbf{y}_\ell^{(k)}\|_\infty$, or

$$\|\mathbf{y}_\ell^{(k+1)}\|_\infty \leq \left(1 + 2nh\alpha\|\mathbf{P}\|_\infty + \frac{h(1+\eta^{(k)})}{n}\right)\|\mathbf{y}_\ell^{(k)}\|_\infty.$$

Whenever $\eta^{(k)}$ and $\max\{\|\mathbf{y}_1^{(k)}\|_\infty, \|\mathbf{y}_2^{(k)}\|_\infty\}$ are bounded by an absolute constant, by setting $r_n = nh\alpha\|\mathbf{P}\|_\infty + \frac{h}{n}$ and assuming $r_n = O(1)$ (by Condition (T1)), we have

$$\|\mathbf{y}_\ell^{(k+1)}\|_\infty \leq (1 + Cr_n)\|\mathbf{y}_\ell^{(k)}\|_\infty, \quad (41)$$

and

$$\begin{aligned} \eta^{(k+1)} &\leq 4 \max_{i \in [n], \ell \in [2]} |y_{i\ell}^{(k)}|^2 \leq 4 \max\{\|\mathbf{y}_1^{(k+1)}\|_\infty^2, \|\mathbf{y}_2^{(k+1)}\|_\infty^2\} \\ &\leq 4(1 + Cr_n) \max\{\|\mathbf{y}_1^{(k)}\|_\infty^2, \|\mathbf{y}_2^{(k)}\|_\infty^2\} = O(1) \end{aligned}$$

In other words, we have shown that for any k such that $\eta^{(k)}$ and $\max\{\|\mathbf{y}_1^{(k)}\|_\infty, \|\mathbf{y}_2^{(k)}\|_\infty\}$ are bounded, then (41) holds, and $\eta^{(k+1)}$ and $\max\{\|\mathbf{y}_1^{(k+1)}\|_\infty, \|\mathbf{y}_2^{(k+1)}\|_\infty\}$ are bounded.

Now Condition (I1) says that $\max\{\|\mathbf{y}_1^{(0)}\|_\infty, \|\mathbf{y}_2^{(0)}\|_\infty\} = O(1)$ and $\eta^{(0)} \leq 4 \max_{\ell \in [2]} \|\mathbf{y}_\ell^{(0)}\|_\infty^2 = O(1)$. By induction, we know that $\eta^{(k)}$ and $\max\{\|\mathbf{y}_1^{(k+1)}\|_\infty, \|\mathbf{y}_2^{(k+1)}\|_\infty\}$ are bounded and (41) holds for all $k \geq 1$. Applying (41) iteratively, we have for any $k \geq 1$,

$$\|\mathbf{y}_\ell^{(k)}\|_\infty \leq (1 + Cr_n)^k \|\mathbf{y}_\ell^{(0)}\|_\infty. \quad (42)$$

Therefore, as long as $k = k(n)$ such that $kr_n = O(1)$ (by Condition (T1)), we have $\frac{\|\mathbf{y}_\ell^{(k)}\|_\infty}{\|\mathbf{y}_\ell^{(0)}\|_\infty} = O(1)$, or

$$\frac{\text{diam}(\{y_i^{(k)}\}_{1 \leq i \leq n})}{\max_{i \in [n], \ell \in [2]} |y_{i\ell}^{(0)}|} \leq \frac{\max_{i \in [n], \ell \in [2]} |y_{i\ell}^{(k)}|}{\max_{i \in [n], \ell \in [2]} |y_{i\ell}^{(0)}|} = O(1).$$

6.3 Proof of Theorem 2

The results concerning (10) and (12) follows directly from Theorem 1 and Proposition 1. To see that (13) holds, we first prove the following proposition.

Proposition 6. *Let $\mathbf{E}_\alpha^{(k)} = \mathbf{S}_\alpha^{(k)} - (\alpha\mathbf{P} - \mathbf{H}_n)$ and $\zeta = \sup_{k \geq 0} \|\mathbf{L}(\mathbf{E}_\alpha^{(k)})\|$. Suppose the initialization satisfies $\|\mathbf{y}_\ell^{(0)}\| \neq 0$ for $\ell = 1, 2$, and (α, h, K) satisfies $h\|\mathbf{L}(\alpha\mathbf{P})\| < 2$, $Kh\zeta = O(1)$ and $Kh = O(n)$ as $n \rightarrow \infty$. Then for $\ell \in \{1, 2\}$, it holds that*

$$\sup_{1 \leq k \leq K} \frac{\|\mathbf{y}_\ell^{(k)} - [\mathbf{I} - h\mathbf{L}(\alpha\mathbf{P} - \mathbf{H}_n)]^k \mathbf{y}_\ell^{(0)}\|_2}{\|\mathbf{y}_\ell^{(0)}\|_2} = O(Kh\zeta). \quad (43)$$

Consequently, for (α, h, k) such that $h\|\mathbf{L}(\alpha\mathbf{P})\| < 2$, $kh\zeta = o(1)$ and $kh = O(n)$, we have

$$\lim_{n \rightarrow \infty} \frac{\|\mathbf{y}_\ell^{(k)} - [\mathbf{I} - h\mathbf{L}(\alpha\mathbf{P} - \mathbf{H}_n)]^k \mathbf{y}_\ell^{(0)}\|_2}{\|\mathbf{y}_\ell^{(0)}\|_2} = 0. \quad (44)$$

By the above proposition, it suffices to reduce the following full list of conditions – $\alpha \gg \frac{1}{n\|\mathbf{P}\|}$, $kh = O(n)$, $nh\alpha\|\mathbf{P}\|_\infty < 1$, $\max_{i \in [n], \ell \in [2]} |y_{i\ell}^{(0)}|^2 = o(\|\mathbf{P}\|/(n\|\mathbf{P}\|_\infty))$, $\|\mathbf{y}_\ell^{(0)}\| \neq 0$ for $\ell \in \{1, 2\}$, $k(nh\alpha\|\mathbf{P}\|_\infty + h/n) = O(1)$, and $k(nh\alpha\|\mathbf{P}\|_\infty + h/n) \cdot \max_{i \in [n], \ell \in [2]} |y_{i\ell}^{(0)}|^2 = O(1)$ – to those in (I1)–(I2) and (T1.D). To see this, note that $k(nh\alpha\|\mathbf{P}\|_\infty + h/n) \cdot \max_{i \in [n], \ell \in [2]} |y_{i\ell}^{(0)}|^2 \rightarrow 0$, can be implied by

$$k(nh\alpha\|\mathbf{P}\|_\infty + h/n) = o(1), \quad \max_{i \in [n], \ell \in [2]} |y_{i\ell}^{(0)}|^2 \ll \|\mathbf{P}\|/(n\|\mathbf{P}\|_\infty) \leq 1.$$

In addition, $kh = O(n)$ and $\alpha hn\|\mathbf{P}\|_\infty < 1$ can be implied by the above first inequality.

6.4 Proof of Theorem 3

Note that $\mathbf{L}(\mathbf{H}_n) = \frac{1}{n-1}\mathbf{I}_n - \frac{1}{n(n-1)}\mathbf{1}_n\mathbf{1}_n^\top$. We have

$$\mathbf{I}_n - h\mathbf{L}(\mathbf{P} - \mathbf{H}_n) = \mathbf{I}_n - h\mathbf{L}(\mathbf{P}) + \frac{h}{n-1}\mathbf{I}_n - \frac{h}{n(n-1)}\mathbf{1}_n\mathbf{1}_n^\top.$$

Without loss of generality, we assume $R \geq 2$, as the case for $R = 1$ follows similarly. Let \mathbf{u}_i be the i -th column of $\mathbf{U}' \in O(n, R-1)$, which consists of the eigenvectors corresponding to the eigenvalue 0 of $\mathbf{L}(\mathbf{P})$ other than the trivial eigenvector $n^{-1/2}\mathbf{1}_n$, and let \mathbf{U} be the matrix that binds an additional column $n^{-1/2}\mathbf{1}_n$ to \mathbf{U}' . Let $\lambda_1 \leq \dots \leq \lambda_n$ be the eigenvalues of $\mathbf{L}(\mathbf{P})$, with $\lambda_1 = \dots = \lambda_R = 0$. Then it follows that

$$\begin{aligned} & \mathbf{I} - h\mathbf{L}(\mathbf{P} - \mathbf{H}_n) \\ &= [\mathbf{U}' \quad n^{-1/2}\mathbf{1}_n \quad \mathbf{U}_\perp] \begin{bmatrix} 1 + \frac{h}{n-1} - h\lambda_1 & & & & & \\ & \ddots & & & & \\ & & 1 + \frac{h}{n-1} - h\lambda_{R-1} & & & \\ & & & 1 + \frac{h}{n-1} - h\lambda_R & & \\ & & & & 1 + \frac{h}{n-1} - h\lambda_{R+1} & \\ & & & & & \ddots \\ & & & & & & 1 + \frac{h}{n-1} - h\lambda_n \end{bmatrix} \\ & \quad \times [\mathbf{U}' \quad n^{-1/2}\mathbf{1}_n \quad \mathbf{U}_\perp]^\top - \frac{h}{n(n-1)}\mathbf{1}\mathbf{1}^\top \\ &= [\mathbf{U}' \quad n^{-1/2}\mathbf{1}_n \quad \mathbf{U}_\perp] \begin{bmatrix} 1 + \frac{h}{n-1} & & & & & & \\ & \ddots & & & & & \\ & & 1 + \frac{h}{n-1} & & & & \\ & & & 1 & & & \\ & & & & 1 + \frac{h}{n-1} - h\lambda_{R+1} & & \\ & & & & & \ddots & \\ & & & & & & 1 + \frac{h}{n-1} - h\lambda_n \end{bmatrix} [\mathbf{U}' \quad n^{-1/2}\mathbf{1}_n \quad \mathbf{U}_\perp]^\top \end{aligned}$$

Then if we denote $\mathbf{u}_{R+1}, \dots, \mathbf{u}_n$ as the columns of \mathbf{U}_\perp , we have

$$(\mathbf{I} - h\mathbf{L}(\mathbf{P} - \mathbf{H}_n))^k = \sum_{i=1}^{R-1} \left(1 + \frac{h}{n-1}\right)^k \mathbf{u}_i \mathbf{u}_i^\top + n^{-1} \mathbf{1} \mathbf{1}^\top + \sum_{i=R+1}^n \left(1 + \frac{h}{n-1} - h\lambda_i\right)^k \mathbf{u}_i \mathbf{u}_i^\top.$$

Hence

$$\begin{aligned} \left\| (\mathbf{I} - h\mathbf{L})^k \mathbf{y} - \left(1 + \frac{h}{n-1}\right)^k \sum_{i=1}^{R-1} \mathbf{u}_i \mathbf{u}_i^\top \mathbf{y} - n^{-1} \mathbf{1} \mathbf{1}^\top \mathbf{y} \right\|_2 &= \left\| \sum_{i=R+1}^n \left(1 + \frac{h}{n-1} - h\lambda_i\right)^k \mathbf{u}_i \mathbf{u}_i^\top \mathbf{y} \right\|_2 \\ &= \sqrt{\sum_{i=R+1}^n \left(1 + \frac{h}{n-1} - h\lambda_i\right)^{2k} (\mathbf{u}_i^\top \mathbf{y})^2} \leq \left(1 + \frac{h}{n-1} - h\lambda_{R+1}\right)^k \|\mathbf{y}\|_2. \end{aligned}$$

the final result follows by noting that $1 + \frac{h}{n-1} - h\lambda_{R+1} < 1 - \kappa/2 < 1$.

6.5 Proof of Proposition 2

Firstly, since \mathbf{A} is nonnegative, by the Geršgorin circle theorem (Varga, 2010), $\mathbf{L}(\mathbf{A})$ is positive semi-definite. For any $\boldsymbol{\theta}_r$, $r \in \{1, \dots, R\}$, it holds that $\mathbf{L}(\mathbf{P})\boldsymbol{\theta}_r = 0$. It follows that $\{\boldsymbol{\theta}_r\}_{r=1}^R$ is a set of eigenvectors corresponding to the smallest eigenvalue 0. In addition, since the graph corresponding to the weighted adjacency matrix \mathbf{P} has R connected components, by the spectral property of the Laplacian matrix (see, for example, Theorem 3.10 of Marsden (2013)), the null space of $\mathbf{L}(\mathbf{P})$ has dimension R . This implies that the eigenvalue 0 of $\mathbf{L}(\mathbf{P})$ has multiplicity R . Lastly, as $\{\boldsymbol{\theta}_k\}_{k=1}^K$ are linearly independent, the eigen subspace associated to the eigenvalue 0 is spanned by $\{\boldsymbol{\theta}_r\}_{r=1}^R$.

6.6 Proof of Theorem 4

Let $\mathbf{E}'_\alpha^{(k)} = \mathbf{S}_\alpha^{(k)} - \alpha \mathbf{P}^* + \mathbf{H}_n$ and $\zeta' = \sup_{k \geq 1} \|\mathbf{L}(\mathbf{E}'_\alpha^{(k)})\|$. Then similar arguments as in the proof of Theorem 2 imply that

$$\boldsymbol{\epsilon}'^{(k)} = \mathbf{y}_\ell^{(k+1)} - (\mathbf{I} - h\mathbf{L}(\alpha \mathbf{P}^* - \mathbf{H}_n))^{k+1} \mathbf{y}_\ell^{(0)},$$

satisfies

$$\frac{\|\boldsymbol{\epsilon}'^{(k)}\|_2}{\|\mathbf{y}_\ell^{(0)}\|_2} \leq (1 + Ch/n)^{k+1} [(1 + h\zeta')^{k+1} - 1].$$

As a result, as long as $h\zeta' \ll 1/k$, we have

$$\lim_{(n,k) \rightarrow \infty} \frac{\|\mathbf{y}_\ell^{(k)} - [\mathbf{I} - h\mathbf{L}(\alpha \mathbf{P}^* - \mathbf{H}_n)]^k \mathbf{y}_\ell^{(0)}\|_2}{\|\mathbf{y}_\ell^{(0)}\|_2} = 0.$$

Now by the inequality $\|\mathbf{L}(\mathbf{A})\| \leq \|\mathbf{D}(\mathbf{A})\| + \|\mathbf{A}\| \leq 2n\|\mathbf{A}\|_\infty$, and the bounded initialization, we have

$$\begin{aligned}\|\mathbf{L}(\mathbf{E}'_\alpha^{(k)})\| &\leq \|\mathbf{L}(\mathbf{S}_\alpha^{(k)} - \alpha\mathbf{P} + \mathbf{H}_n)\| + \alpha\|\mathbf{L}(\mathbf{P}^* - \mathbf{P})\| \\ &\leq 2n\|\mathbf{S}_\alpha^{(k)} - \alpha\mathbf{P} + \mathbf{H}_n\|_\infty + \alpha\|\mathbf{L}(\mathbf{P}^* - \mathbf{P})\| \\ &\leq (\alpha n\|\mathbf{P}\|_\infty + 1/n) \cdot \max_{i \in [n], \ell \in [2]} |y_{i\ell}^{(0)}|^2 + \alpha\|\mathbf{L}(\mathbf{P}^* - \mathbf{P})\|\end{aligned}\quad (45)$$

where the last inequality follows from Proposition 1. Thus, the condition $h\zeta' \ll 1/k$ can be implied by

$$k[(nh\alpha\|\mathbf{P}\|_\infty + h/n) \cdot \max_{i \in [n], \ell \in [2]} |y_{i\ell}^{(0)}|^2 + \alpha h\|\mathbf{L}(\mathbf{P}^* - \mathbf{P})\|] = o(1),$$

which can be satisfied by Conditions (I2) (T1.D) and (T2.D). Now, if we further assume $\kappa < h\lambda_{R+1}(\mathbf{L}(\alpha\mathbf{P}^*)) \leq h\|\mathbf{L}(\alpha\mathbf{P}^*)\| \leq 1$ and $k \rightarrow \infty$, by Theorem 3, we also have

$$\lim_{(n,k) \rightarrow \infty} \frac{\|\mathbf{y}_\ell^{(k)} - \mathbf{U}\mathbf{U}^\top \mathbf{y}_\ell^{(0)}\|_2}{\|\mathbf{y}_\ell^{(0)}\|_2} = 0,$$

where the columns of $\mathbf{U} \in O(n, R-1)$ span the null space of $\mathbf{L}(\mathbf{P}^*)$. By Proposition 2, we know that the matrix $\mathbf{U}\mathbf{U}^\top \begin{bmatrix} \mathbf{y}_1^{(0)} & \mathbf{y}_2^{(0)} \end{bmatrix} \in \mathbb{R}^{n \times 2}$ has at most R distinct rows, and any two rows corresponding to the same graph component in G have the identical values. Then, the final results follow by setting $\{z_1, \dots, z_R\}$ such that $z_r = (z_{1r}, z_{2r})$ is the same as the rows in $\mathbf{U}\mathbf{U}^\top \begin{bmatrix} \mathbf{y}_1^{(0)} & \mathbf{y}_2^{(0)} \end{bmatrix}$ corresponding to the r -th graph component.

References

Amini, A. A. and Z. S. Razaee (2019). Concentration of kernel matrices with application to kernel spectral clustering. *arXiv preprint arXiv:1909.03347*.

Arora, S., W. Hu, and P. K. Kothari (2018). An analysis of the t-SNE algorithm for data visualization. In *Conference on Learning Theory*, pp. 1455–1462. PMLR.

Balakrishnan, S., M. Xu, A. Krishnamurthy, and A. Singh (2011). Noise thresholds for spectral clustering. In *Advances in Neural Information Processing Systems*, pp. 954–962.

Belkin, M. and P. Niyogi (2003). Laplacian eigenmaps for dimensionality reduction and data representation. *Neural Computation* 15(6), 1373–1396.

Carreira-Perpinán, M. A. (2010). The elastic embedding algorithm for dimensionality reduction. In *ICML*, Volume 10, pp. 167–174.

Chatzimparmpas, A., R. M. Martins, and A. Kerren (2020). t-viSNE: Interactive assessment and interpretation of t-SNE projections. *IEEE Transactions on Visualization and Computer Graphics* 26(8), 2696–2714.

Cheng, J., H. Liu, F. Wang, H. Li, and C. Zhu (2015). Silhouette analysis for human action recognition based on supervised temporal t-SNE and incremental learning. *IEEE Transactions on Image Processing* 24(10), 3203–3217.

Donoho, D. (2017). 50 years of data science. *Journal of Computational and Graphical Statistics* 26(4), 745–766.

Gisbrecht, A., A. Schulz, and B. Hammer (2015). Parametric nonlinear dimensionality reduction using kernel t-SNE. *Neurocomputing* 147, 71–82.

Hinton, G. and S. T. Roweis (2002). Stochastic neighbor embedding. In *Advances in Neural Information Processing Systems*, Volume 15, pp. 833–840.

Im, D. J., N. Verma, and K. Branson (2018). Stochastic neighbor embedding under f-divergences. *arXiv preprint arXiv:1811.01247*.

Jacobs, R. A. (1988). Increased rates of convergence through learning rate adaptation. *Neural Networks* 1(4), 295–307.

Kobak, D. and P. Berens (2019). The art of using t-SNE for single-cell transcriptomics. *Nature Communications* 10(1), 1–14.

Kruskal, J. B. (1978). *Multidimensional Scaling*. Number 11. Sage.

Linderman, G. C., M. Rachh, J. G. Hoskins, S. Steinerberger, and Y. Kluger (2019). Fast interpolation-based t-SNE for improved visualization of single-cell rna-seq data. *Nature Methods* 16(3), 243–245.

Linderman, G. C. and S. Steinerberger (2019). Clustering with t-SNE, provably. *SIAM Journal on Mathematics of Data Science* 1(2), 313–332.

Lui, K., G. W. Ding, R. Huang, and R. McCann (2018). Dimensionality reduction has quantifiable imperfections: Two geometric bounds. In *Advances in Neural Information Processing Systems*, Volume 31, pp. 8453–8463.

Marsden, A. (2013). Eigenvalues of the laplacian and their relationship to the connectedness of a graph.

Moon, K. R., D. van Dijk, Z. Wang, S. Gigante, D. B. Burkhardt, W. S. Chen, K. Yim, A. van den Elzen, M. J. Hirn, R. R. Coifman, et al. (2019). Visualizing structure and transitions in high-dimensional biological data. *Nature biotechnology* 37(12), 1482–1492.

Olivon, F., N. Elie, G. Grelier, F. Roussi, M. Litaudon, and D. Touboul (2018). Metgem software for the generation of molecular networks based on the t-SNE algorithm. *Analytical Chemistry* 90(23), 13900–13908.

Pezzotti, N., B. P. Lelieveldt, L. Van Der Maaten, T. Höllt, E. Eisemann, and A. Vilanova (2016). Approximated and user steerable tSNE for progressive visual analytics. *IEEE Transactions on Visualization and Computer Graphics* 23(7), 1739–1752.

Platzer, A. (2013). Visualization of snps with t-SNE. *PLoS One* 8(2), e56883.

Schölkopf, B., A. Smola, and K.-R. Müller (1997). Kernel principal component analysis. In *International Conference on Artificial Neural Networks*, pp. 583–588. Springer.

Shaham, U. and S. Steinerberger (2017). Stochastic neighbor embedding separates well-separated clusters. *arXiv preprint arXiv:1702.02670*.

Traven, G., G. Matijević, T. Zwitter, M. Žerjal, J. Kos, M. Asplund, J. Bland-Hawthorn, A. R. Casey, G. De Silva, K. Freeman, et al. (2017). The galah survey: classification and diagnostics with t-SNE reduction of spectral information. *The Astrophysical Journal Supplement Series* 228(2), 24.

van der Maaten, L. (2014). Accelerating t-SNE using tree-based algorithms. *The Journal of Machine Learning Research* 15(1), 3221–3245.

van der Maaten, L. and G. Hinton (2008). Visualizing data using t-SNE. *Journal of Machine Learning Research* 9(Nov), 2579–2605.

Varga, R. S. (2010). *Geršgorin and his circles*, Volume 36. Springer Science & Business Media.

Venna, J., J. Peltonen, K. Nybo, H. Aidos, and S. Kaski (2010). Information retrieval perspective to nonlinear dimensionality reduction for data visualization. *Journal of Machine Learning Research* 11(2).

Wang, Y., H. Huang, C. Rudin, and Y. Shaposhnik (2020). Understanding how dimension reduction tools work: An empirical approach to deciphering t-SNE, umap, trimap, and pacmap for data visualization. *arXiv preprint arXiv:2012.04456*.

Xie, B., Y. Mu, D. Tao, and K. Huang (2011). m-SNE: Multiview stochastic neighbor embedding. *IEEE Transactions on Systems, Man, and Cybernetics, Part B (Cybernetics)* 41(4), 1088–1096.

Yang, Z., I. King, Z. Xu, and E. Oja (2009). Heavy-tailed symmetric stochastic neighbor embedding. In *Advances in Neural Information Processing Systems*, Volume 22, pp. 2169–2177.

Zhang, Y. and S. Steinerberger (2021). t-SNE, forceful colorings and mean field limits. *arXiv preprint arXiv:2102.13009*.